npj | biofilms and microbiomes

Article

Published in partnership with Nanyang Technological University

https://doi.org/10.1038/s41522-026-00923-x

Simiao Decoction alleviates hyperuricemia-induced renal injury through regulating gut dysbiosis and decreasing gut-derived uremic toxins

Xinghong Zhou[1,2,3,4,6], Xiaoyu Liu[3,6], Baizhao Peng[1,2,3,6], Ying Yang[1,2,3,6], Hanqi Lu[4], Dexian Li[1,2,3], Yijian Deng[2,3], Zihao Jiang[2,3], Chuanghai Wu[2,3], Wen Fang[2,3], Yanting You[2,3], Hiu Yee Kwan[5], Xiaoshan Zhao[1,2,3] ✉ & Yanyan Liu[2] ✉

Renal injury is a common complication of hyperuricemia (HUA), which has been recognized as an independent risk factor for chronic kidney disease (CKD). The gut-kidney axis theory suggests that targeting the gut microbiota may be a potential treatment option for kidney disease. In this study, we utilized a spontaneous HUA rat model to demonstrate that Simiao decoction (SMD), a traditional Chinese medicine formula, can effectively alleviate HUA-induced renal injury by modulating gut microbiota and bacterial metabolism of tryptophan and tyrosine, thereby reducing gut-derived uremic toxins such as indoxyl sulfate (IS) and p-Cresol (PC). Fecal microbiota transplantation (FMT) further confirmed that the therapeutic effect of SMD was mediated by gut microbiota. Finally, in vitro studies revealed that IS promotes epithelial-mesenchymal transition (EMT) while PC induces cellular senescence in tubular cells. Collectively, our findings suggest that SMD can effectively alleviate HUA-induced renal injury through regulating gut dysbiosis and decreasing gut-derived uremic toxins. This study sheds light on a novel mechanism by which SMD exerts its effects on HUA-induced renal injury.

Hyperuricemia (HUA) is a common metabolic disorder. The global prevalence of HUA is gradually increasing. The overall hyperuricemia prevalence in China has risen from 11.1% in 2015–2016 to 14.0% in 2018–2019, a significant rise was observed in the three years[1]. In addition to its primary association with gout, HUA is closely linked to other conditions, including type 2 diabetes[2], hypertension[3], cardiovascular diseases[4] and chronic kidney disease (CKD)[5]. The kidney functions are frequently affected by HUA. HUA is regarded as an independent risk factor for CKD[6]. The mechanisms through which HUA leads to renal injury include the induction of tubular damage, inflammation, and tubulointerstitial fibrosis[7,8].

The gut-kidney axis theory well illustrates the vital role of gut microbiota on kidney health[9]. Increasing studies suggest that gut microbiota and their metabolites serve as essential mediators of the gut-kidney axis, significantly contributing to the maintenance of renal health[10,11]. Gut dysbiosis is closely linked to the progression of renal pathologies[12,13]. Additionally, substantial differences in gut microbiota composition have been observed between individuals with HUA and healthy controls, in both humans and rodents[14,15]. Our previous study provides additional insights into the role of gut dysbiosis in exacerbating renal injury in HUA rats[15], indicating that therapeutic interventions targeting the modulation of intestinal microbiota could offer a promising approach for treating HUA-related renal injury.

Overproduction and inadequate excretion of uric acid (UA) are the two primary pathological factors for HUA. The therapeutic approach for HUA and HUA-related diseases aims to reduce UA production and/or promote its excretion. Xanthine oxidase inhibitors, such as allopurinol and febuxostat, are capable of decreasing uric acid production, while uricosuric agents like benzbromarone and probenecid increase UA excretion. These are the main effective UA-lowering agents used in clinical practice[16]. However, their clinical application is hindered by the significant adverse effects. For example, allopurinol has been reported to frequently cause renal damage

[1]Nanfang Hospital, Southern Medical University, Guangzhou, Guangdong, China. [2]School of Traditional Chinese Medicine, Southern Medical University, Guangzhou, Guangdong, China. [3]Guangdong Basic Research Center of Excellence for Integrated Traditional and Western Medicine for Qingzhi Diseases, Guangzhou, China. [4]Dongguan Hospital of Guangzhou University of Chinese Medicine, Dongguan, China. [5]School of Chinese Medicine, Hong Kong Baptist University, Hong Kong, China. [6]These authors contributed equally: Xinghong Zhou, Xiaoyu Liu, Baizhao Peng, Ying Yang. ✉e-mail: zhaoxs@smu.edu.cn; 799042406@qq.com

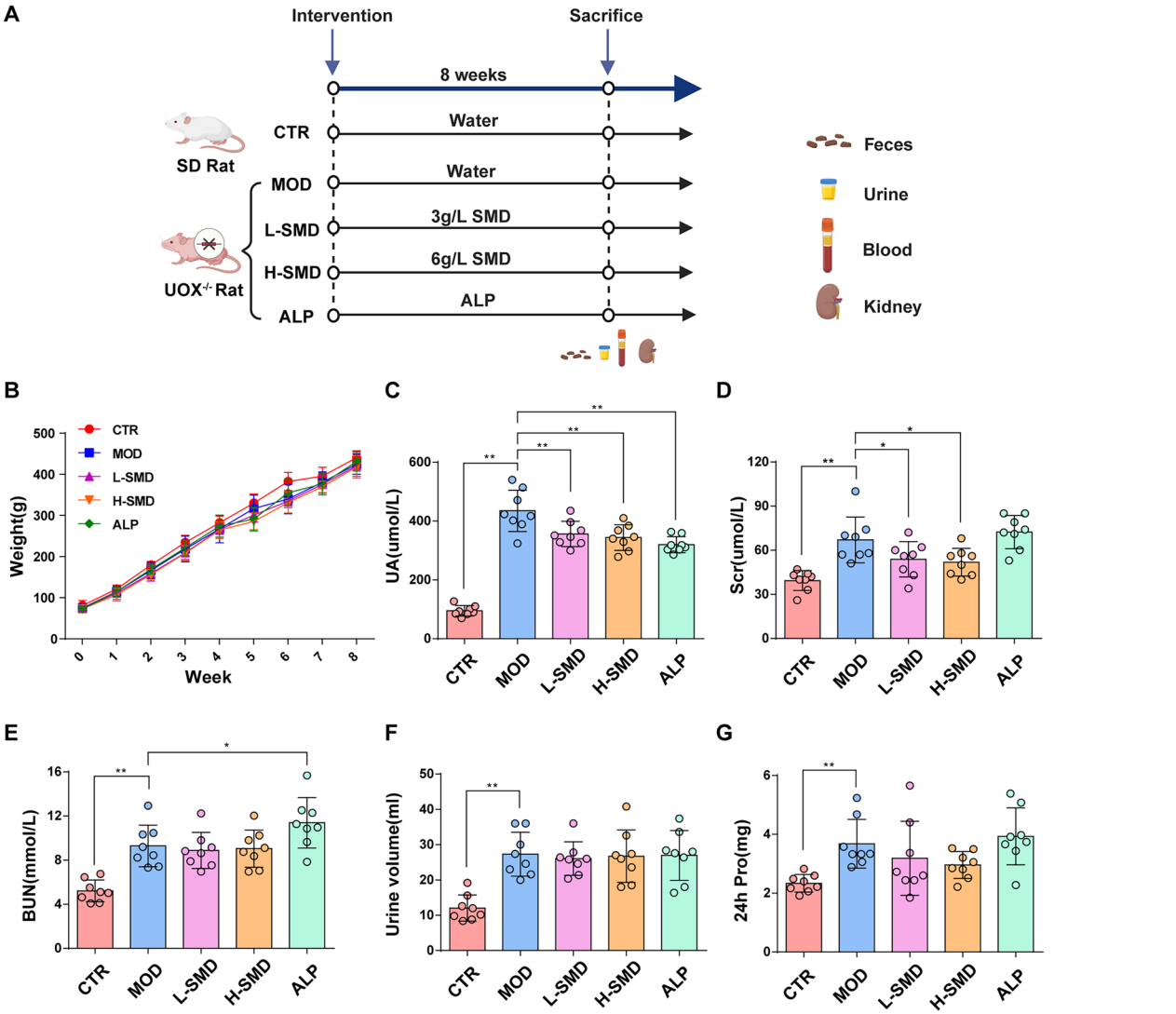

Fig. 1 | SMD alleviates HUA and renal dysfunction in the UOX$^{-/-}$ rats. **A** The scheme of the experiment. **B** Body weight changes ($n = 8$). **C** Serum UA concentrations of different groups ($n = 8$). **D** Scr concentrations of different groups ($n = 8$). **E** BUN concentrations of different groups ($n = 8$). **F** Urine volume level of different groups ($n = 8$). **G** 24-h urine proteins level of different groups ($n = 8$). Data are represented as mean ± SD. Statistical comparison was performed using One-way ANOVA followed by the post hoc LSD tests. $^{*}p < 0.05$, $^{**}p < 0.01$.

and Stevens-Johnson syndrome, while probenecid may lead to neurodegeneration[17–19]. Therefore, there remains a need to develop effective agents with fewer side effects.

Chinese herbal medicines are evidence-based therapies with proven efficacy and acceptable safety for the treatment of HUA and HUA-related diseases[20,21]. Simiao decoction (SMD) is a classic traditional Chinese medicine formula used to treat HUA and HUA-related diseases[22,23]. Previous studies have demonstrated that SMD can mitigate HUA and HUA-induced renal injury in mice by inhibiting inflammation, apoptosis, and renal fibrosis[24,25]. However, the involvement of intestinal microbiota in the protective effects of SMD on HUA-induced renal injury and the underlying mechanisms are not fully understood.

The limited research on the impact of SMD on HUA-induced gut dysbiosis may be attributed to the absence of a stable HUA model. It is well known that HUA is a chronic metabolic disease, drug-induced acute HUA model may be not suitable for the study of HUA-induced microbiota change and the effects of SMD. The inactivation of the uricase gene in primate evolution predisposes humans to HUA. The uricase (UOX) gene encodes uricase, which degrades UA to allantoin in the rodent liver, posing a challenge for establishing stable HUA animal models. HUA models are typically established by administering drugs that either enhance purine synthesis or inhibit uricase activity. Nevertheless, the instability of serum UA levels in drug-induced models makes them inadequate for HUA research, especially for the study of HUA-induced gut dysbiosis. Therefore, in this study, an UOX-knockout (UOX$^{-/-}$) rat model was ultilized to investigate the nephroprotective effects of SMD on HUA and reveal the underlying mechanisms.

Results

UPLC-MS/MS analysis of SMD

SMD is composed of 4 herbs, as detailed in Table S1. A total of 59 components were identified using UPLC/MS/MS in both positive and negative ion modes (Fig. S1). These components included berberine, ferulic acid, baicalin, gallic acid, citric acid, and others. The specific characteristic fragments of the 59 compounds are enumerated in Table S2.

SMD alleviates HUA and renal dysfunction in the UOX$^{-/-}$ rats

The experiment design was shown in Fig. 1A, UOX$^{-/-}$ rats were randonly divided into model (MOD) group, low-dose SMD (L-SMD) group, high-dose SMD (H-SMD) group and allopurinol (ALP) group, while wild-type

rats were assigned to control (CTR) group. Blood, urine, feces and kideneys were collected after 8 weeks intervention. As seen in Fig. 1B and Fig. S2A, body weight and food intake showed no significant differences across the groups. However, compared to wild-type rats, water intake was markedly increased in UOX$^{-/-}$ rats, and neither SMD nor ALP treatment had any effect on the water intake of intake of UOX$^{-/-}$ rats (Fig. S2B). As expected, serum UA levels of UOX$^{-/-}$ rats were significantly higher than wildtype rats (Fig. 1C), indicating successful establishment of the HUA model. Additionally, the UOX$^{-/-}$ rats displayed obvious renal dysfunction, as evidenced by elevated Scr, BUN and 24-hour urine proteins (Fig. 1D–G). After 8 weeks of treatment, both SMD and ALP effectively reduced serum UA levels in the UOX$^{-/-}$ rats. Furthermore, both L-SMD and H-SMD group demonstrated significant reduction in Scr levels in the UOX$^{-/-}$ rats (Fig. 1D), suggesting nephroprotective properties against HUA-induced kidney injury. Unexpectedly, ALP not only failed to alleviate renal dysfunction but rather aggravated it, as indicated by elevated BUN levels in the UOX$^{-/-}$ rats.

To investigate whether SMD treatment could induce hepatotoxicity in rats, histopathological H&E staining of rat liver tissue was performed. Histological analysis revealed no discernible alterations in hepatic tissue across the various rat groups (Fig. S3A). Additionally, no statistically significant differences were observed in serum AST and ALT levels across the groups (Fig. S3B). In total, these results indicate that SMD alleviates HUA and renal dysfunction in the UOX$^{-/-}$ rats without causing obvious hepatotoxicity.

SMD attenuates renal histopathological injury in the UOX$^{-/-}$ rats

To provide more comprehensive analysis of the kidney injury induced by HUA and the protective effect of SMD, we conducted examinations of kidney gross morphology and histopathology. As shown in Fig. 2A, compared to wildtype rats, UOX$^{-/-}$ rats developed evident impairment of kidney morphology with less smooth surface and severe structural damage, which were attenuated by SMD treatment. The presence of UA crystals observed in UOX$^{-/-}$ rats was significantly reduced by different doses of SMD and ALP treatment (Fig. 2B). H&E staining results revealed that SMD treatment mitigated renal tubule dilatation, disorganized epithelial cell arrangement, and inflammatory cell infiltration induced by HUA in the kidneys of UOX$^{-/-}$ rats (Fig. 2C). Furthermore, PAS staining results demonstrated that tubular injury in the HUA rat kidneys, characterized by tubular dilation, detached epithelial cells, and damage to the brush border membrane within tubular lumens, was ameliorated following different doses of SMD administration (Fig. 2D–F). Consistent with PAS staining results, levels of several biomarkers for tubular injury increased in the urine of UOX$^{-/-}$ rats, including urinary NAGL and KIM-1, all significantly reduced in H-SMD group (Fig. 2G–H). However, ALP not only failed to alleviate but rather aggravated tubular injury, as indicated by elevated KIM-1, RBP, and β2-MG levels in urine samples from UOX$^{-/-}$ rats (Fig. 2G, I and J). In summary, these findings suggest that SMD could mitigate HUA-induced renal histopathological injuries especially those related to renal tubules. Our results also indicate the potential nephrotoxicity associated with long-term use of ALP. Additionally, according to the results of tubular injury biomarkers, we found that H-SMD group showed a better renoprotective effect than L-SMD group in HUA rats. Therefore, H-SMD group was chosen to explored the mechanism of SMD on the effects of HUA-induced renal injury.

SMD alleviates renal fibrosis in the UOX$^{-/-}$ rats

Renal fibrosis is a prevalent pathological characteristic in various CKD. To investigate this, we conducted Masson trichrome staining and collagen III immunohistochemical staining. As depicted in Fig. 3A–D, UOX$^{-/-}$ rats exhibited significantly higher kidney collagen accumulation than wildtype rats. However, treatment with SMD resulted in a notable reduction of collagen accumulation in the kidneys of UOX$^{-/-}$ rats.

Epithelial-mesenchymal transition (EMT) constitutes a fundamental process in the pathogenesis of renal interstitial fibrosis. Several biomarkers are utilized to characterize EMT, with epithelial cells predominantly expressing E-cadherin, while mesenchymal cells express N-cadherin and α-SMA. Additionally, TGF-β/Smad2 plays a significant role in the induction of EMT. As depicted in Fig. 3E–G, compared to wildtype rats, there was a reduction in E-cadherin protein expression, whereas the expressions of N-cadherin, α-SMA, TGF-β, and Smad2 were elevated in the kidneys of UOX$^{-/-}$ rats. In contrast, high dose SMD treatment notably upregulated E-cadherin expression and downregulated N-cadherin, α-SMA, TGF-β and Smad2 expression in the kidneys of UOX$^{-/-}$ rats. In total, these results suggest that SMD alleviates renal fibrosis in UOX$^{-/-}$ rats.

SMD reduces inflammation and cellular senescence in the kidneys of UOX$^{-/-}$ rats

Chronic inflammation represents a common pathological feature of HUA, where NLRP3 inflammasome activation significantly contributes to renal inflammation and fibrosis progression. Immunohistochemical staining for CD68 revealed a higher macrophage count in the kidneys of UOX$^{-/-}$ rats (Fig. 4A). The serum concentrations of IL-1β, IL-6, and MCP-1 (Fig. 4C–E), as well as the protein expressions of IL-1β, cleaved-caspase 1, and NLRP3 (Fig. 4F and G), were consistently elevated in the kidneys of UOX$^{-/-}$ rats. Conversely, different doses of SMD treatment significantly reduced the serum levels of IL-6, IL-1β and MCP-1, as well as the protein expression of IL-1β, cleaved-caspase 1, and NLRP3 in the kidneys of UOX$^{-/-}$ rats.

Cellular senescence is intricately linked to renal fibrosis development. To investigate whether HUA could induce cellular senescence in the kidney and the effects of SMD, Sa-β-gal staining was conducted. The results of Sa-β-gal staining showed a significant increase in cell senescence in the kidneys of UOX$^{-/-}$ rats (Fig. 4B). Interestingly, the positive area of Sa-β-gal staining mainly focused on the renal tubule. Additionally, Western blot results also revealed an up-regulation of cell senescence-related protein expression, including P16^{INK4A} and P21, in the kidneys of UOX$^{-/-}$ rats compared to wildtype rats (Fig. 4H and I). Conversely, SMD treatment significantly reduced both the positive area of Sa-β-gal staining and the renal protein expression levels of P16^{INK4A} and P21 in UOX$^{-/-}$ rats. Collectively, these findings suggest that SMD treatment has the potential to reduce inflammation and cellular senescence in the kidneys of UOX$^{-/-}$ rats.

SMD improves intestinal barrier and regulates gut dysbiosis in the UOX$^{-/-}$ rats

The intestinal barrier plays a crucial role in preventing the transfer of endogenous and exogenous antigens, as well as pathogenic microorganisms, from the intestinal tract to the systemic circulation, thus ensuring the health of animals. Therefore, we first investigated the effects of SMD on the intestinal barrier function of UOX$^{-/-}$ rats. H&E and AB staining of colonic tissues revealed an impairment of the intestinal barrier, characterized by a thinner mucus layer and damage to colonic crypts (Fig. 5A, B and D). Additionally, morphological observations of intestinal tight junctions by TEM showed a impairment of intestinal barrier in UOX$^{-/-}$ rats (Fig. 5C). Consistent with these findings, colonic protein expressions of ZO-1 and occludin were decreased in UOX$^{-/-}$ rats (Fig. 5E and F). In contrast, treatment with SMD was found to improve the intestinal barrier function in UOX$^{-/-}$ rats by repairing the structure of colonic crypts, promoting mucus excretion, and upregulating expression levels of tight junction proteins.

The gut microbiota is essential for the kidney health maintenance. A metagenomic analysis was conducted to assess SMD's effect on the gut microbiota in HUA rats. The α-diversity indices, including the Shannon and Chao1 indices, demonstrated comparable microbial richness and evenness between the MOD and SMD groups (Fig. 6A and B). A principal coordinates analysis (PCoA) using Bray-Curtis distance revealed distinct differences in microbial community composition between the two groups (Fig. 6C). At the phylum level, Firmicutes, Bacteroidetes and Proteobacteria were identified as the main bacteria in both MOD and SMD groups, with no significant differences in abundance observed for Firmicutes and Bacteroidetes between the two groups (Fig. 6D–F, Fig. S4A). At the species level, several species include potential probiotics and pathogenic bacteria were identified (Fig. S4B). LEfSe analysis was further performed to identify microbial biomarkers at species level for each group (Fig. 6G). The results

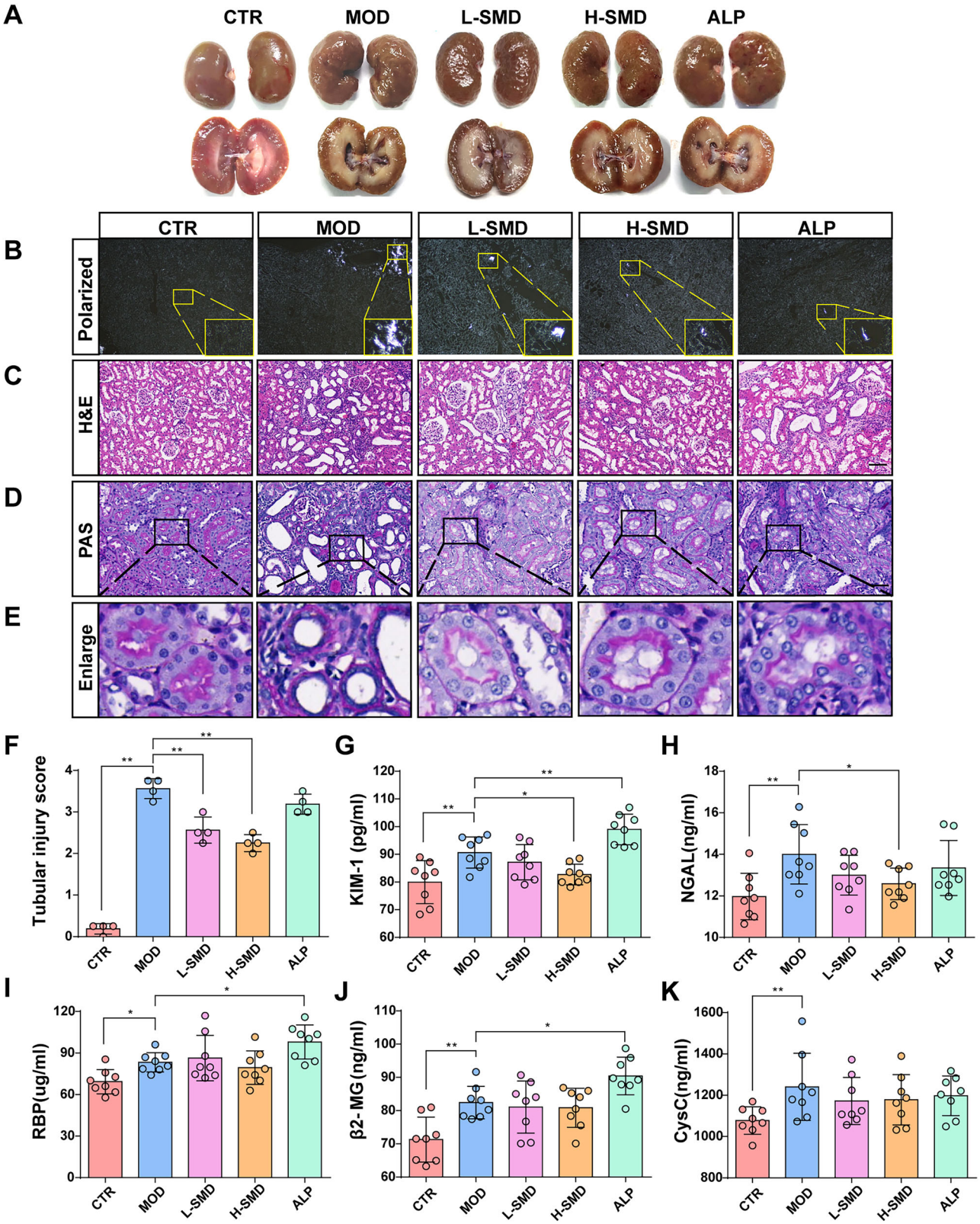

Fig. 2 | SMD attenuates renal histopathological injury in the UOX$^{-/-}$ rats. **A** Kidney morphology of different groups. **B** UA crystals detected under polarized light in the kidneys of rats. **C** Representative kidney H&E staining of different groups. Scale bar, 100 μm. **D–F** Representative kidney PAS staining and renal tubular injury scores of different groups ($n = 4$). Scale bar, 50 μm. **G–K** Urinary KIM-1, NGAL, RBP, β2-MG, and CysC concentrations of different groups ($n = 8$). Data are represented as mean ± SD. Statistical comparison was performed using One-way ANOVA followed by the post hoc LSD tests. $^{*}p < 0.05$, $^{**}p < 0.01$.

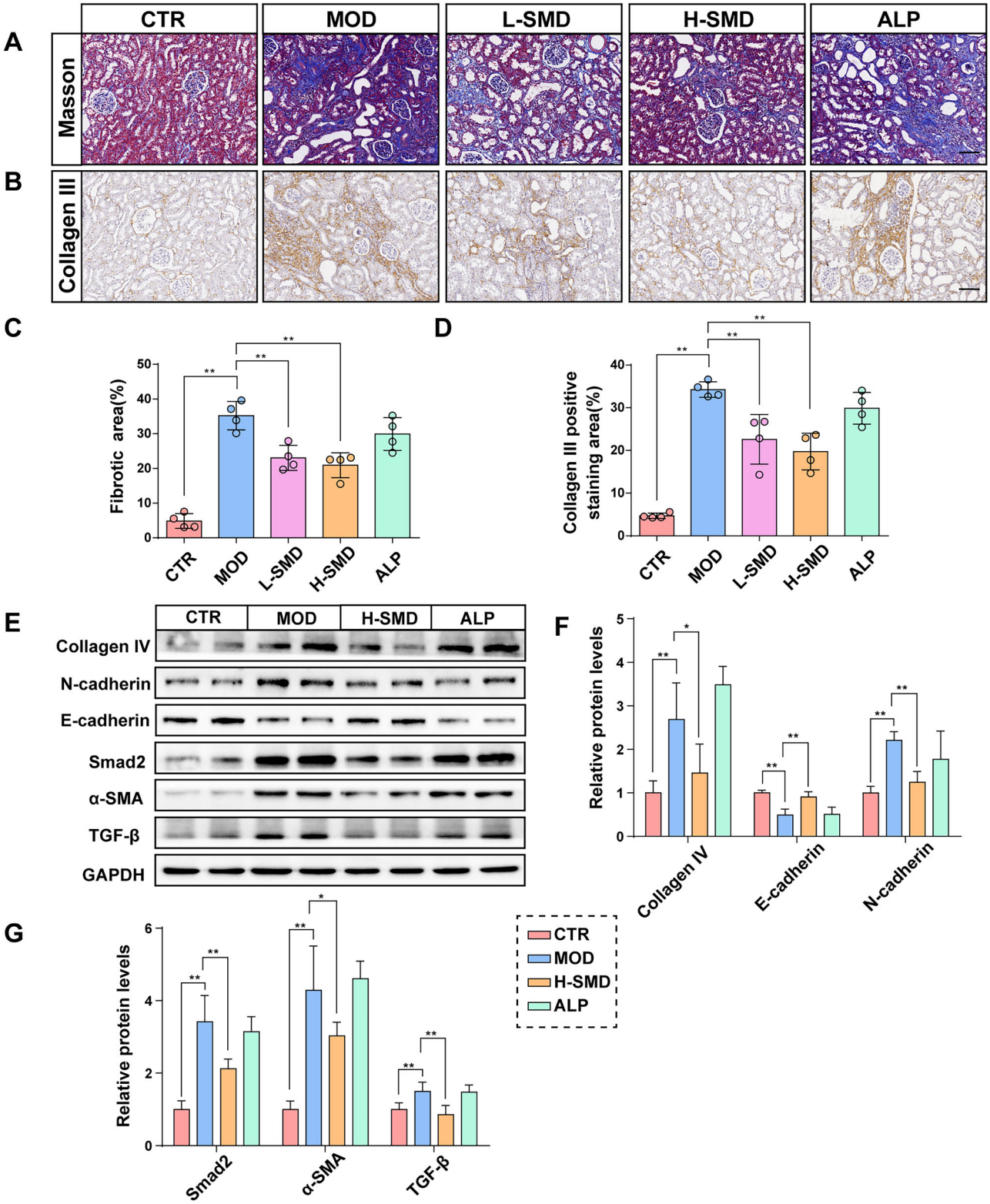

Fig. 3 | SMD alleviates renal fibrosis in the UOX$^{-/-}$ rats. A Representative kidney masson trichrome staining of different groups ($n = 4$). Scale bar, 100 μm. **B** Representative immunohistochemistry staining for Collagen III ($n = 4$). Scale bar, 100 μm. **C** Quantification of masson trichrome staining positive areas ($n = 4$). **D** Quantification of Collagen III immunohistochemistry staining ($n = 4$). Scale bar, 100 μm. **E–G** Representative western blot and quantification of Collagen IV, N-cadherin, E-cadherin, Smad2, α-SMA and TGF-β proteins in the kidneys of rats ($n = 4$). Data are represented as mean ± SD. Statistical comparison was performed using One-way ANOVA followed by the post hoc LSD tests. $^{*}p < 0.05$, $^{**}p < 0.01$.

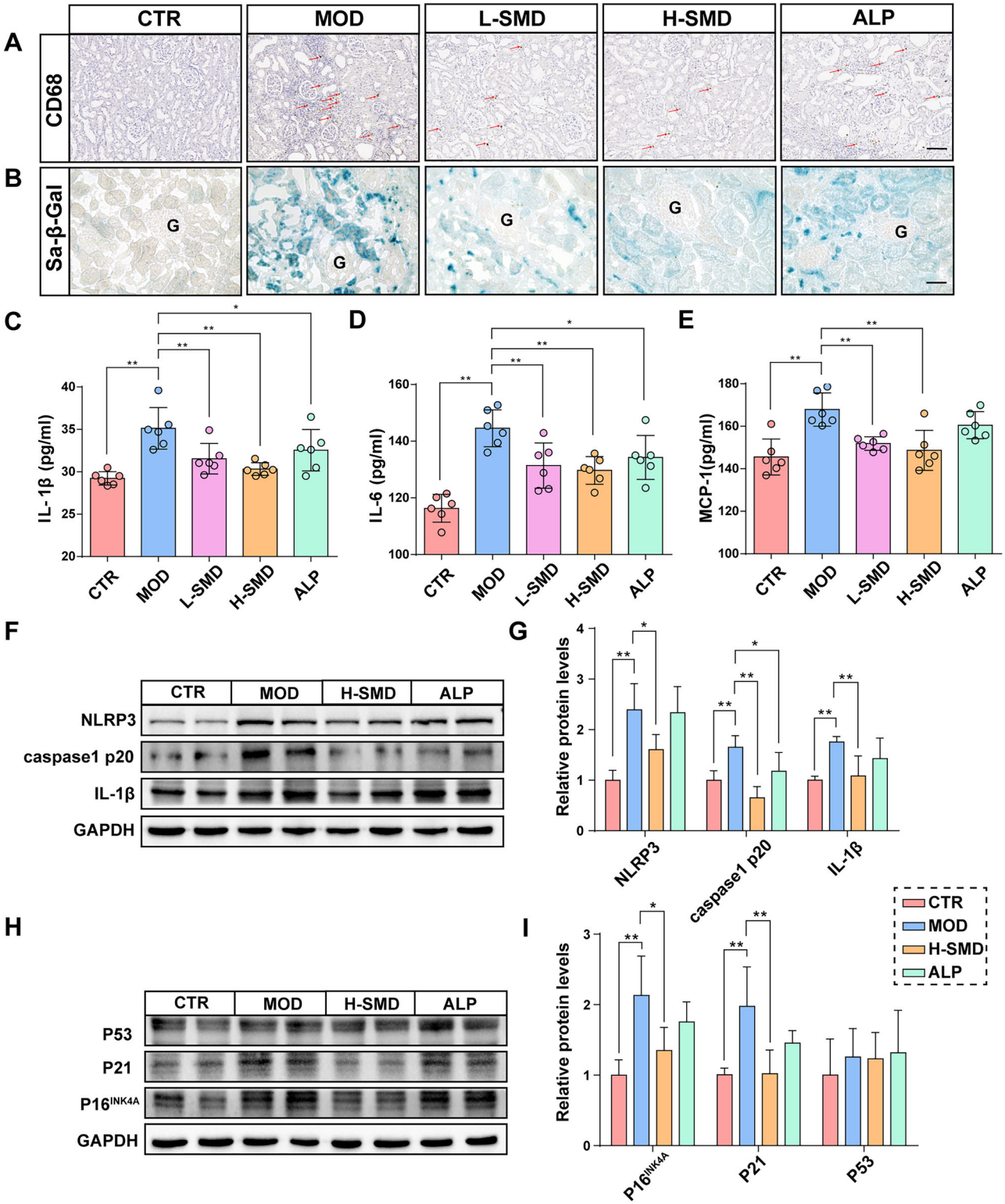

Fig. 4 | SMD inhibits inflammation and cellular senescence in the kidneys of UOX$^{-/-}$ rats. A Representative immunohistochemistry staining for CD68. Red arrows indicate CD68-positive macrophage. Scale bar, 100 μm. **B** Representative kidney Sa-β-gal staining of different groups. G means glomerulus. Scale bar, 50 μm. **C** Serum IL-1β concentrations of different groups ($n = 6$). **D** Serum IL-6 concentrations of different groups ($n = 6$). **E** Serum MCP-1 concentrations of different groups ($n = 6$). **F**, **G** Representative western blot and quantification of NLRP3, caspase1 p20 and IL-1β proteins in the kidneys of rats ($n = 4$). **H**, **I** Representative western blot and quantification of P53, P21 and P16^{INK4A} proteins in the kidneys of rats ($n = 4$). Data are represented as mean ± SD. Statistical comparison was performed using One-way ANOVA followed by the post hoc LSD tests. $^{*}p < 0.05$, $^{**}p < 0.01$.

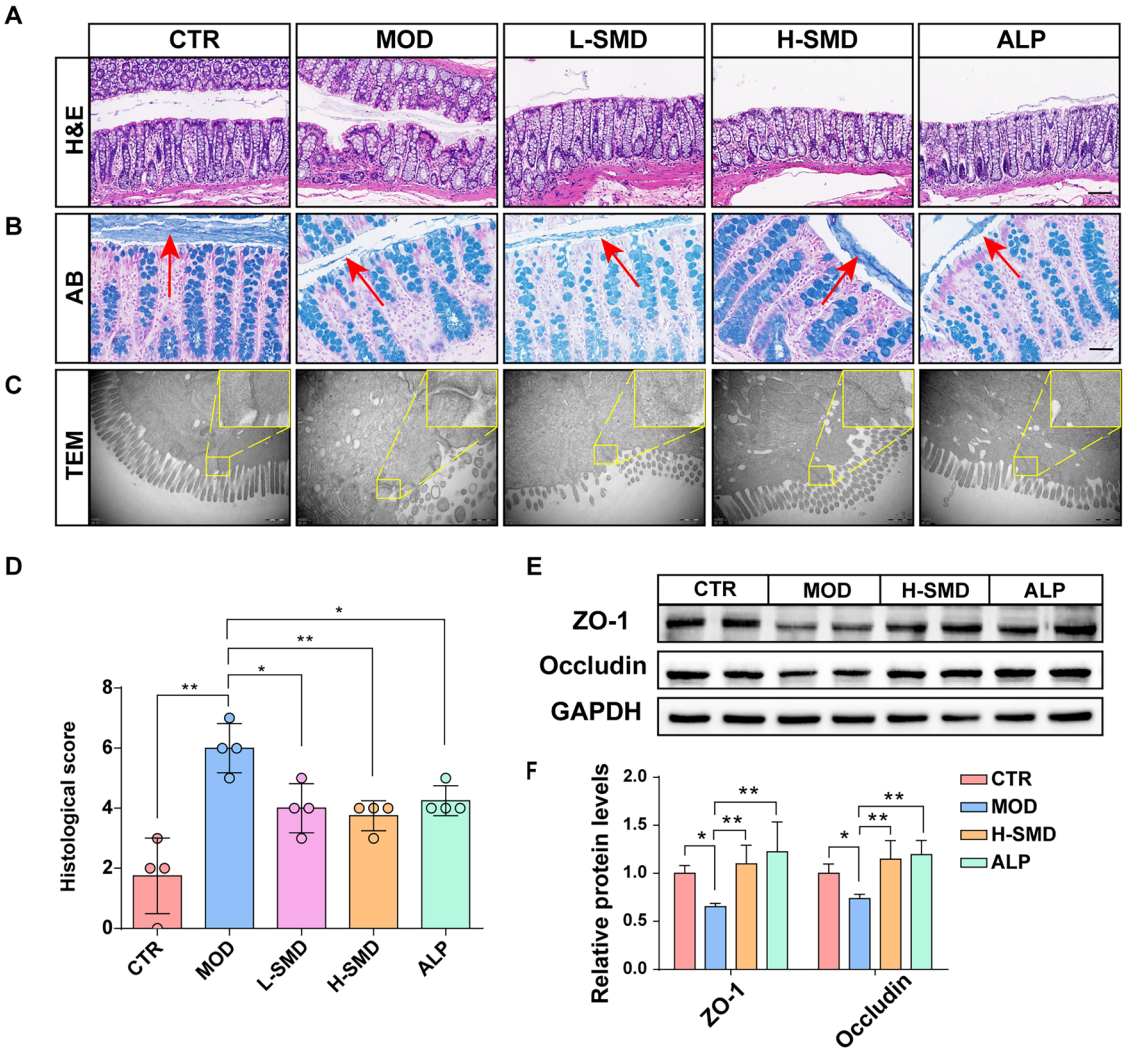

Fig. 5 | SMD improves intestinal barrier in the UOX$^{-/-}$ rats. A Representative colon H&E staining of different groups. Scale bar, 100 μm. **B** Representative colon AB staining of different groups. Scale bar, 50 μm. Mucus layer was indicated by red arrow. **C** Representative colon TEM of different groups. Scale bar, 500 nm. **D** Histological score of colon ($n = 4$). **E**, **F** Representative western blot and quantification of ZO-1 and occludin proteins in the kidneys of rats ($n = 4$). Data are represented as mean ± SD. Statistical comparison was performed using One-way ANOVA followed by the post hoc LSD tests. $^{*}p < 0.05$, $^{**}p < 0.01$.

showed an enrichment of 6 potential probiotics, including *Muribaculum_gordoncarteri, Lactobacillus_intestinalis, Prevptella_copri* and *Lactococcus_lactis*, in the SMD group, while 2 potential pathogenic bacteria, including *Eschericha_coli* and *Lactobacillus_taiwanensis*, were enriched in the MOD group (Fig. 6H and I). Additionally, Pearson correlation analysis revealed that that *Lactobacillus_taiwanensis* enriched in MOD group was positively correlated with renal dysfunction parameters such as KIM-1 and NGAL, whereas *Prevotella_copri* and *Lactococcus_lactis* enriched in SMD group were negatively correlated with renal dysfunction parameters (Fig. 6J). Collectively, these findings clearly indicated that SMD significantly enhanced the function of the intestinal barrier and modulated the gut microbiota in HUA rats.

SMD regulates the metabolism of gut microbiota in the UOX$^{-/-}$ rats

Metagenomic analysis indicated that SMD modulated the gut microbiota structure and composition in UOX$^{-/-}$ rats. To further investigate the effects of SMD on the metabolism of gut microbiota in HUA rats, fecal untargeted metabolomic analysis was performed. As depicted in Fig. 7A, the OPLS-DA model results demonstrated a distinct separation between the SMD and MOD groups, indicating differences in microbiota metabolites between the two groups. A 200-iteration random permutation test validated the OPLS-DA model's robustness (Fig. S5A). After filtering by VIP > 1 and $p < 0.05$, a total of 28 metabolites were identified between the SMD and MOD groups (Fig. 7B), with 13 metabolites up-regulated and 15 down-regulated in SMD group. Of particular interest among these altered microbiota metabolites is indole, a precursor of multiple uremic toxins derived from tryptophan metabolism by gut microbiota. Consistently, enriched KEGG pathway analysis indicated that tryptophan metabolism by microbiota was down-regulated in the SMD group (Fig. 7C). Pearson correlation results showed that *Escherichia-coli* enriched in MOD group were positively correlated with indole and other differential metabolites, whereas *Muribaculum_gordoncarteri, Lactobacillus_intestinalis* enriched in SMD group were negatively correlated with these altered metabolites (Fig. 7D).

These results reveal that SMD potentially modulates gut microbiota metabolism, notably by suppressing tryptophan metabolism. This effect could be beneficial in alleviating HUA-induced kidney injury.

SMD inhibits the production of gut-derived uremic toxins in the UOX$^{-/-}$ rats

The results of fecal metabolomic analysis indicated that SMD could inhibit the tryptophan metabolism of gut microbiota, leading to a reduction in the production of indole and other harmful microbial metabolites. However, it remains unclear whether these metabolites could enter the bloodstream and

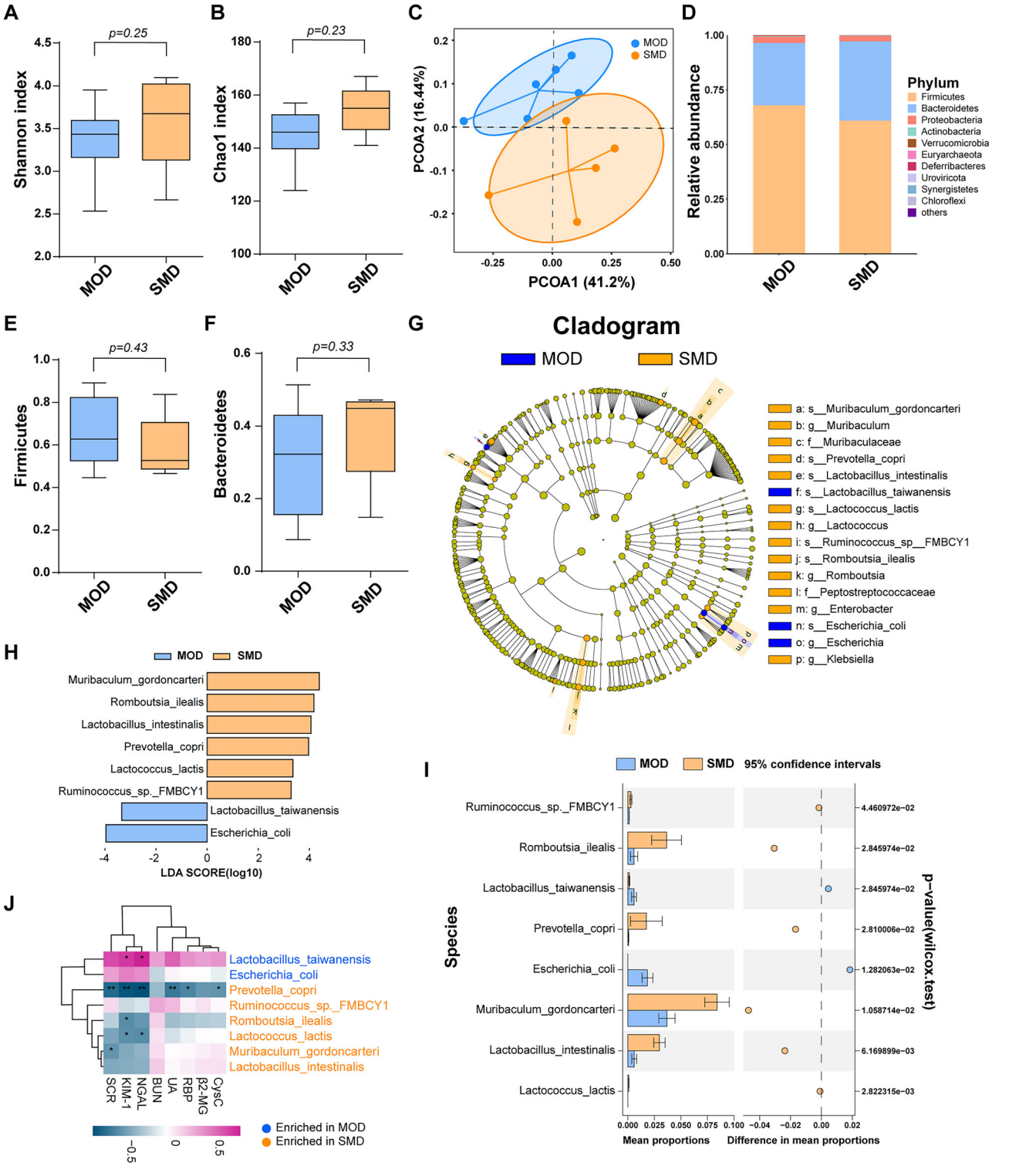

Fig. 6 | SMD regulates gut dysbiosis in the UOX−/− rats. A Shannon index ($n = 5–6$). **B** Chao1 index ($n = 5–6$). **C** PCoA analysis using Bray-Curtis distances between MOD and SMD groups ($n = 5–6$). **D** Relative abundance profiles at the phylum level ($n = 5–6$). **E** Relative abundance of Firmicutes ($n = 5–6$). **F** Relative abundance of Bacteroidetes ($n = 5–6$). **G** Cladogram of LEfSe analysis. **H** Biomarker species and their LDA scores between MOD and SMD groups ($n = 5–6$). **I** Relative abundance of different species between MOD and SMD groups. **J** Pearson correlation between differential species and renal injury parameters. Data are represented as mean ± SD. Statistical comparison was performed using Wilcox rank-sum tests.

be further metabolized by the host, ultimately resulting in the production of uremic toxins that may impair kidney function. To address this question, a targeted metabolomics analysis of kidney tissues was performed. As depicted in Fig. 8A, the OPLS-DA model results demonstrated a distinct separation between the SMD and MOD groups, suggesting differences in microbiota metabolites between the two groups. A 200-iteration random permutation test validated the OPLS-DA model's robustness (Fig. S5B).

After filtering by VIP > 1 and $p < 0.05$, 127 kidney metabolites were identified between the SMD and MOD groups (Fig. S6), with 25 metabolites up-regulated and 102 down-regulated in the SMD group. These metabolites

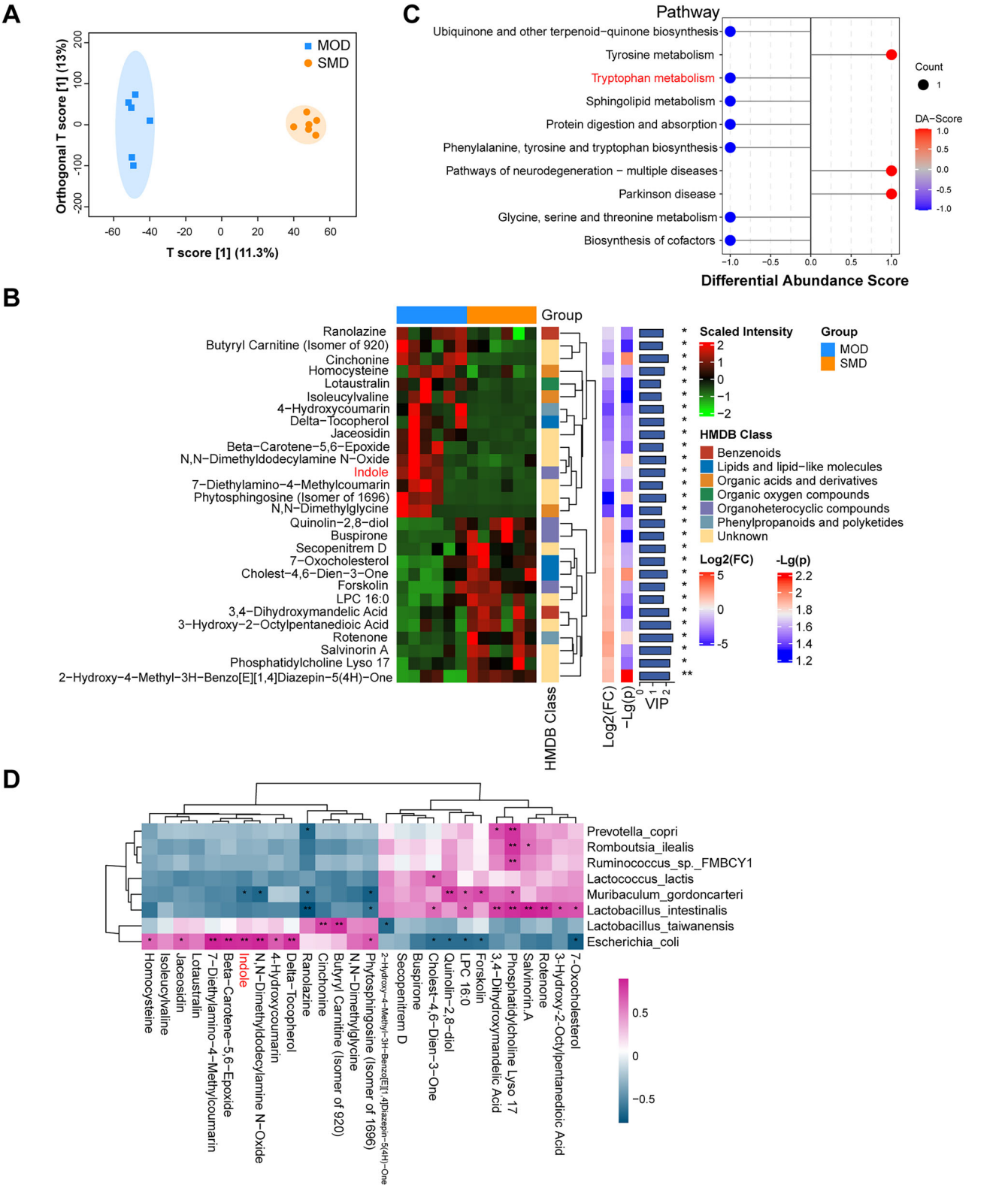

Fig. 7 | SMD regulates the metabolism of gut microbiota in the UOX$^{-/-}$ rats. **A** OPLS-DA model discrimination based on metabolic profiles in fecal samples between MOD and SMD groups ($n = 6$). **B** Complex heatmap of differential metabolites between MOD and SMD groups ($n = 6$). **C** Differential abundance score of the KEGG pathway between MOD and SMD groups. **D** Pearson correlation between differential species and metabolites. $^{*}p < 0.05$, $^{**}p < 0.01$.

primarily include amino acids, nucleosides, nucleotides, and analogues, peptides, and analogues, organic acids and derivatives, phosphatidyl acids, indoles and heterocyclic compounds (Fig. 8B). KEGG enrichment analysis showed that the tyrosine metabolism and other pathways were down-regulated in SMD group (Fig. 8C). Among these, several uremic toxins including lipoxin A4, methylguanidine, indoxyl sulphate (IS) and p-Cresol (PC), were down-regulated after SMD treatment (Fig. 8D). It's well known that IS and PC are common uremic toxins derived from gut bacteria

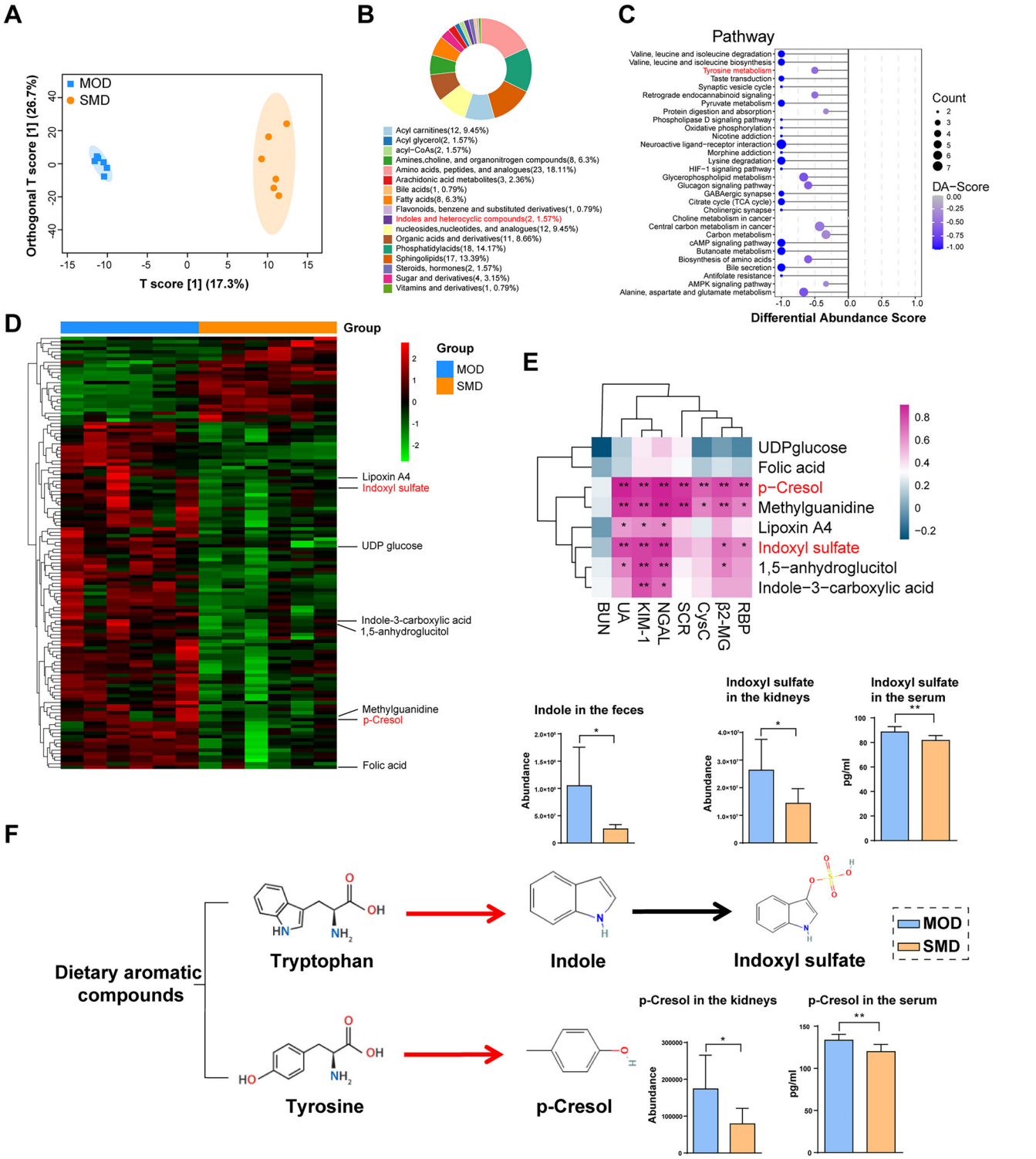

Fig. 8 | SMD inhibits the production of gut-derived uremic toxins in the UOX$^{-/-}$ rats. **A** OPLS-DA model discrimination based on metabolic profiles in kidney samples between MOD and SMD groups ($n = 6$). **B** Classification of differential metabolites between MOD and SMD groups. **C** Differential abundance score of the KEGG pathway between MOD and SMD groups. **D** Heatmap of differential metabolites between MOD and SMD groups. **E** Pearson correlation between differential metabolites in the kidneys of rats and renal injury parameters. **F** The production and relative abundance of IS and PC in MOD and SMD groups ($n = 6$). Red arrows indicate processes mediated by gut microbes while black arrows indicate processes mediated by host. Data are represented as mean ± SD. Statistical comparison was performed using two-tailed unpaired Student's *t* tests. $^{*}p < 0.05$; $^{**}p < 0.01$.

(Fig. 8F). Correlation analysis also showed that IS and PC were positively correlated with renal function parameters (Fig. 8E).

These data suggest that SMD inhibits the production of gut-derived uremic toxins in UOX$^{-/-}$ rats, thereby alleviating HUA-induced kidney injury.

Gut microbiota mediates the protective effects of SMD on renal injury

The results of multi-omics analysis suggest that the gut microbiota may mediate the renal protective effects of SMD. To test our hypothesis, fecal

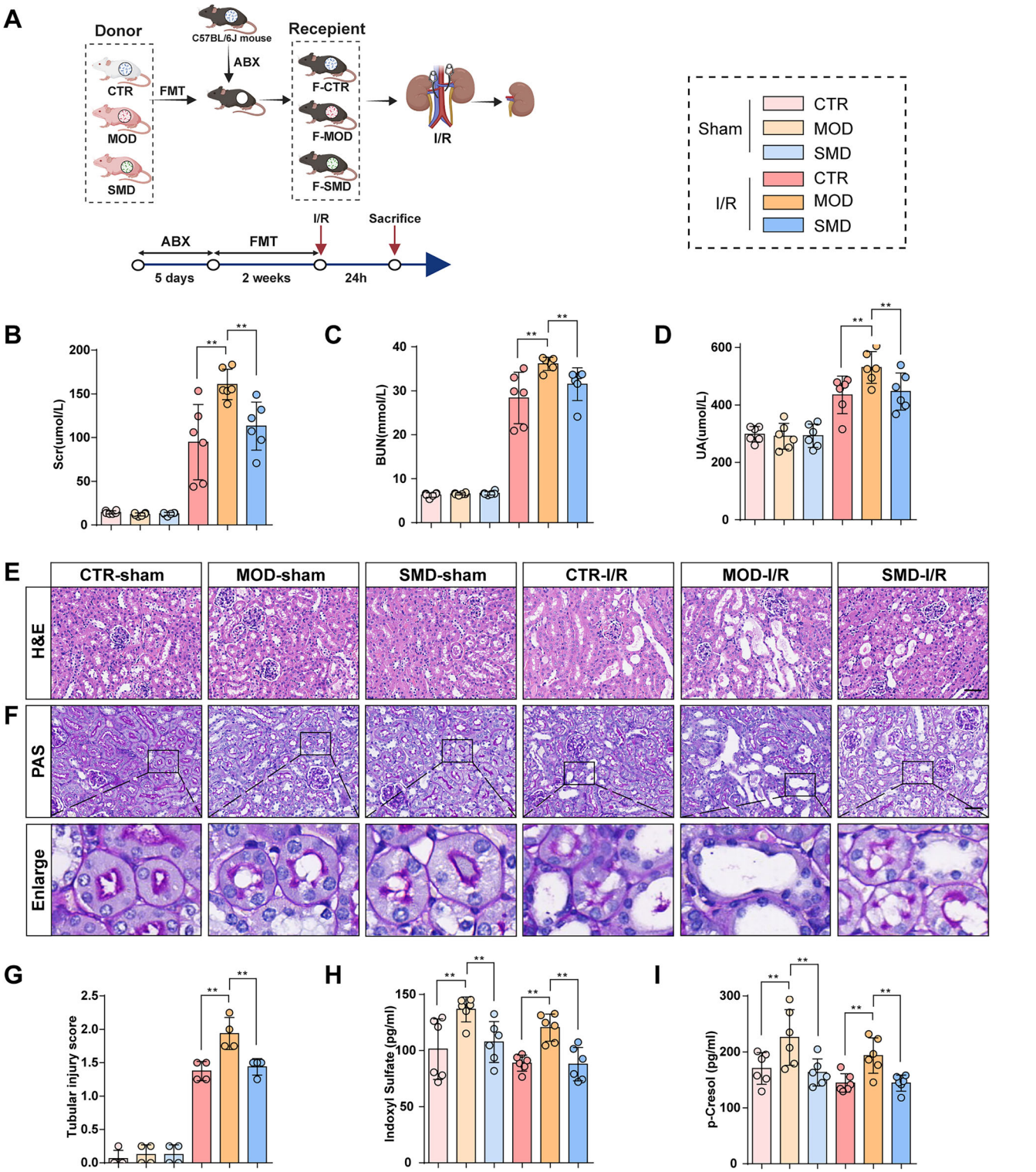

Fig. 9 | Gut microbiota mediates the protective effects of SMD on renal injury. **A** The schedule of FMT and I/R surgery. FMT fecal microbiota transplantation, I/R ischemia/reperfusion, ABX antibiotic. **B**–**D** Levels of Scr, BUN and UA in recipient mice ($n = 6$). **E**, **F** H&E and PAS staining of kidneys in recipient mice. Scale bar, 50 μm. **G** Renal tubular injury scores ($n = 4$). **H**, **I** Levels of IS and PC in recipient mice ($n = 6$). Data are represented as mean ± SD. Statistical comparison was performed using One-way ANOVA followed by the post hoc LSD tests. $^{**}p < 0.01$.

microbiota was transplanted from CTR, MOD and H-SMD group rats into gut microbiota-depleted mice for two weeks. Subsequently, ischemia/reperfusion (I/R) surgery was performed in the recipient mice to induce acute renal injury (Fig. 9A). As shown in Fig. 9B–D, no differences were observed in Scr, BUN or UA when comparing HUA microbiota recipient mice to control mice, or when comparing them to SMD microbiota recipient mice, indicating that the HUA microbiota might not directly induce renal injury. However, HUA microbiota recipient mice following the I/R surgery showed an increase in Scr, BUN and UA levels when compared to the control group, while SMD microbiota recipient mice showed a significantly decrease Scr, BUN and UA levels when compared to HUA microbiota recipient mice after I/R surgery. Consistently, renal

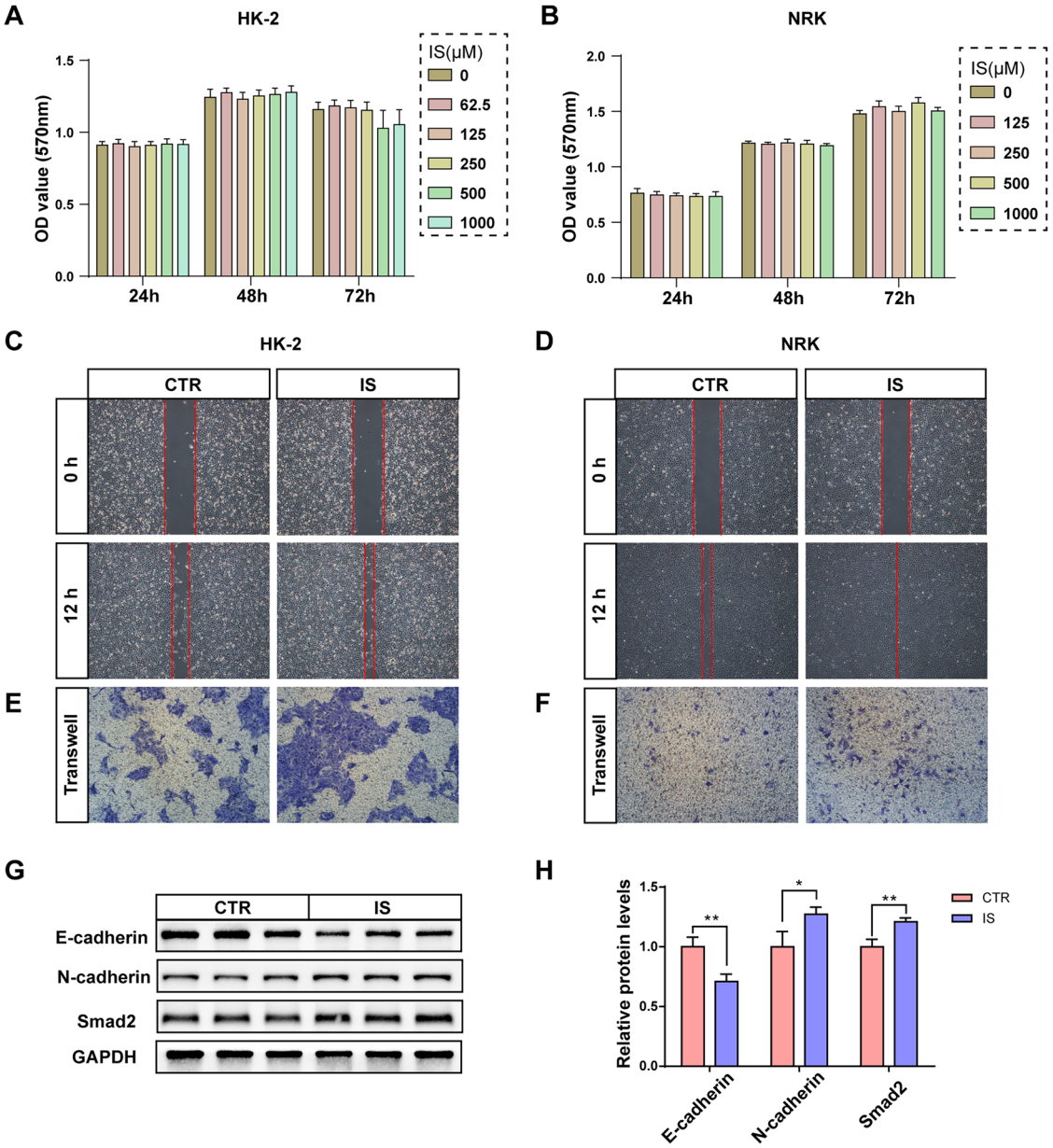

Fig. 10 | IS promotes EMT in renal tubular epithelial cells. A, **B** Effects of IS (62.5, 125, 250, 500 and 1000 μM) on HK-2 and NRK-52E cells viability. **C**, **D** Microscopy images of HK-2 and NRK-52E cell migration scratch assay. **E**, **F** Microscopy images of transwell migration of HK-2 and NRK-52E cells. **G**, **H** Representative western blot and quantification of N-cadherin, E-cadherin and Smad2, proteins in NRK-52E cells ($n = 3$). Data are represented as mean ± SD. Statistical comparison was performed using two-tailed unpaired Student's t tests. $^{*}p < 0.05$; $^{**}p < 0.01$.

tubular injury was ameliorated in SMD microbiota recipient mice when compared to HUA microbiota recipient mice after I/R surgery (Fig. 9E–G). Moreover, the serum levels of IS and PC, two key gut-derived uremic toxins obsereved in metablomic analyses, were significantly down-regulated in SMD microbiota recipient mice compared to HUA microbiota recipient mice after I/R surgery (Fig. 9H and I). These results suggest that gut microbiota mediates the protective effects of SMD on HUA-induced renal injury.

IS and PC promotes EMT and cellular senescence in renal tubular epithelial cells, respectively

The results of the kidney metabolomic analysis and FMT revealed that SMD may inhibit the production of uremic toxins derived from gut bacteria (IS and PC) in UOX$^{-/-}$ rats, thereby alleviating HUA-induced kidney injury. To further investigate the underlying mechanism, HK-2 and NRK-52E cells were treated with IS and PC.

According to the MTT assay results, IS did not influence the proliferation of either HK-2 or NRK-52E cells (Fig. 10A and B). However, transwell and scratch assays showed that IS could significantly increase the migratory and invasive capacity of HK-2 and NRK-52E cells (Fig. 10C–F). Increased migratory and invasive capacity are the characteristic of EMT. Western blot analysis further demonstrated that IS led to a down-regulation in the protein expression levels of E-cadherin, while concurrently up-regulating the protein expression levels of N-cadherin and Smad2 (Fig. 10G and H). These findings suggest that IS induces EMT in the renal tubular epithelial cells.

Furthermore, the MTT results demonstrated that PC inhibited the cell viability of HK-2 and NRK-52E cells (Fig. 11A and B). PC treatment reduced the numbers of viable HK-2 and NRK-52E cells and induced cellular senescence as indicated by a characteristic large and flattened morphology (Fig. 11C and D). The Sa-β-gal staining results indicated that PC facilitated the senescence of renal tubular cells (Fig. 11E and F).

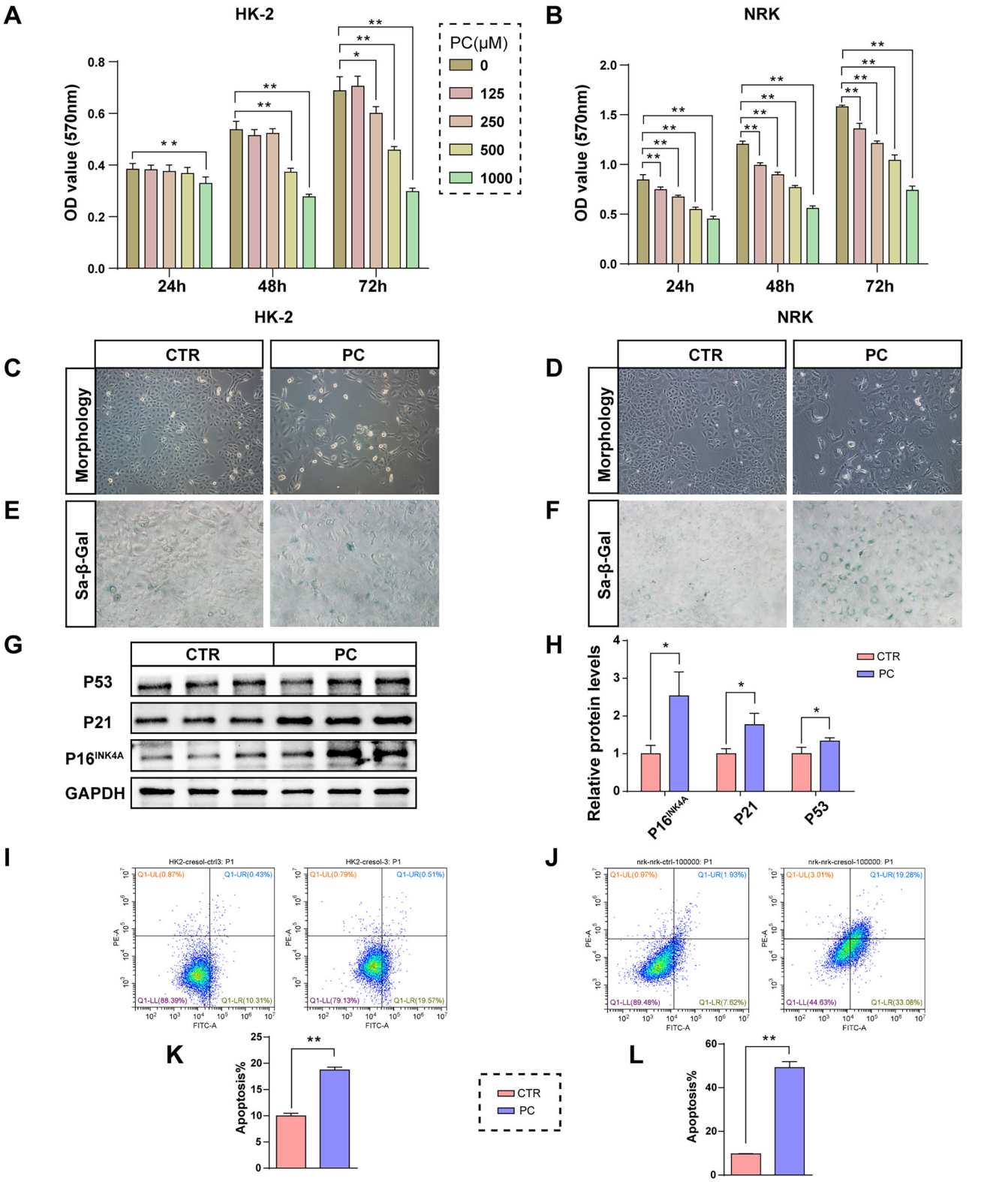

Fig. 11 | PC promotes renal tubular cell senescence and apoptosis. A, **B** Effects of PC (0, 125, 250, 500 and 1000 μM) on HK-2 and NRK-52E cells viability. **C**, **D** Microscopy images of HK-2 and NRK-52E cell morphology. **E**, **F** Representative images of SA-β-gal staining of HK-2 and NRK-52E cells. **G**, **H** Representative western blot and quantification of P53, p21 and $P16^{INK4A}$ proteins in NRK-52E cells ($n = 3$). **I**, **J** Representative images of HK-2 and NRK-52E cellular apoptosis detected by flow cytometry. **K**, **L** Quantification of apoptosis rate of HK-2 and NRK-52E cells. Data are represented as mean ± SD. Statistical comparison was performed using two-tailed unpaired Student's *t* tests. $^{*}p < 0.05$; $^{**}p < 0.01$.

Correspondingly, Western blot analysis demonstrated that PC treatment led to an upregulation in the expression of senescence-associated proteins, such as $P16^{INK4A}$, P21, and P53 (Fig. 11G and H). Additionally, PC induced apoptosis in renal tubular cells (Fig. 11I–L), suggesting that it induces both senescence and apoptosis in the cells.

Discussion

HUA is closely related to kidney diseases. And HUA animal models are crucial for HUA-related disease research. In this study, a spontaneous HUA rat model with UOX gene knockout was utilized. Our results indicate that SMD significantly alleviates HUA-induced renal injury in $UOX^{-/-}$ rat model. The protective effects of SMD may attributed to its regulation of gut dysbiosis and enhancement of intestinal barrier function, leading to a reduction in gut-derived uremic toxins and the inhibition of EMT, cellular senescence, and apoptosis in renal tubular cells.

Traditional chinese medicine (TCM) offer distinct benefits in improving symptoms associated with HUA, minimizing toxic side effects, and reducing the likelihood of disease recurrences. As a classic prescription in China, SMD has been widely utilized for treating HUA and its associated complications. While animal studies have validated the therapeutic effects of SMD in HUA-related renal injury, the underlying mechanism remains unclear. Therefore, this study employed a $UOX^{-/-}$ rat model to further investigate the efficacy and mechanism of SMD. As anticipated, $UOX^{-/-}$ rats displayed spontaneous HUA and obvious renal injury. Both SMD and ALP demonstrated their ability to lower uric acid levels in $UOX^{-/-}$ rats. However, when compared to ALP, SMD exhibited distinct advantages in protecting against HUA-induced renal injury. This advantage was confirmed through pathological staining and detection of renal tubular injury markers. Notably, ALP not only failed to alleviate tubular injury but also exacerbated the process, indicating the adverse effects on renal function with prolonged use of ALP.

Renal fibrosis represents the ultimate common pathway resulting from diverse renal injuries, culminating in CKD and end-stage renal disease. EMT is considered the key mechanism underlying renal fibrosis. The anti-fibrotic effects of SMD on the kidneys of $UOX^{-/-}$ rats were confirmed by Masson staining and Western blot analysis. Additionally, cellular senescence, characterized by stress-induced irreversible growth arrest, is implicated in the progression of renal disease. The acceleration of tubular cell senescence exacerbates the pathogenesis of renal fibrosis[26,27]. Senescent cells can be detected through SA-β-gal staining, and these cells exhibit a loss of proliferative and reparative capacities. Additionally, they secrete elements characteristic of the senescence-associated secretory phenotype (SASP), which includes proinflammatory cytokines such as IL-1β, IL-6 and MCP-1, as well as pro-fibrotic mediators like TGF-β1[28,29]. In this study, apparent tubular senescence was observed in the kidneys of HUA rats using SA-β-gal staining. Furthermore, SMD significantly inhibited tubular senescence and the secretion of proinflammatory cytokines.

The gut microbiota and their metabolites are closely associated with the occurrence and development of kidney disease. Our previous study found that gut dysbiosis induced by HUA could promote renal injury in $UOX^{-/-}$ rats, suggesting that targeting the microbiota may be an effective strategy for treating HUA-related renal injury[15]. Therefore, metatgenomic was performed firstly to test the effects of SMD on gut microbiota in HUA rats. Our study demonstrated a notable disparity in the structure and composition of gut microbiota through PcoA analysis and bacteria abundance analysis. The LEfSe analysis revealed several potential probiotics that were significantly enriched in the SMD group. These included *Lactobacillus_intestinalis*, *Prevotella_copri*, and *Lactococcus_lactis*. In contrast, Eschericha_*coli*, a common opportunistic pathogenic bacteria, was found to be enriched in the MOD group. Previous studies have shown that *Lactobacillus_intestinalis* is reduced in CKD rats[30], while *Prevotella_copri* has been found to mediate the beneficial effects of therapeutic food for malnutrition[31]. Additionally, *Lactococcus lactis* is recognized as a safe microorganism for regulating intestinal micro-ecological balance and improving immune performance[32]. Furthermore, it is crucial to emphasize that the *Escherichia coli* genome harbors genes encoding tryptophanase, an enzyme that facilitates the conversion of tryptophan into indole, which can subsequently be metabolized into IS. This suggests a potential role for *Escherichia coli* in the production of uremic toxin[14,33]. Therefore, the protective effects of SMD on HUA-induced renal injury may be related to the upregulation of *Lactobacillus_intestinalis, Prevotella_copri* and *Lactococcus_lactis* and the downregulation of *Eschericha_coli*.

After conducting gut metagenomic analysis, we proceeded with fecal metabolomic analysis to further explore the regulation of SMD on gut microbiota in HUA rats. Among these differential metabolites, our attention was drawn to the decrease in indole in the SMD group, as it is a product of microbiota tryptophan metabolism and a precursor of IS. Consistently, the results of metabolite-enriched KEGG pathway revealed the regulatory effect of SMD on microbiota tryptophan metabolism. In addition to IS, quinolinic acid (QA), L-kynurenine (KYN) and kynurenic acid (KA) are also uremic toxins derived from the metabolism of tryptophan by the gut microbiota. These results suggest that SMD inhibits the tryptophan metabolism of gut microbiota to alleviate HUA-induced renal injury. However, whether indole and other differential metabolites could enter the bloodstream and be further metabolized to uremic toxins by the host to impact renal function remains unknown. To address this question, kidney metabolic analysis was performed. In line with the results of fecal metabolomics analysis, IS abundance in the kidneys of HUA rats was significantly reduced by SMD. Additionally, PC, another common uremic toxin produced from tyrosine metabolism by intestinal anaerobic bacteria[13], was also reduced in the kidneys of SMD group. The results of metabolite-enriched KEGG pathway also indicated the inhibition of SMD on tyrosine metabolism. Both IS and PC are protein-bound uremic toxins that cannot be efficiently cleared by hemodialysis; therefore, regulation of gut microbiota may contribute to reducing uremic toxins and alleviating renal injury. Moreover, our recent studies found that IS and PC were accumulated in $UOX^{-/-}$ rat kidneys[15]. These results suggest that SMD alleviates HUA-induced renal injury by regulating gut microbiota to reduce the production of uremic toxins, including IS and PC. Interestingly, berberine, the main component in SMD identified by UPLC-MS/MS, has been reported to ameliorate CKD by modulating the gut microbiota and suppressing the synthesis of gut-derived uremic toxins, including PC[34]. This provides additional evidence for the regulatory effects of SMD on the gut-kidney axis.

FMT study confirmed that the therapeutic effects of SMD was mediated through modulation of the gut microbiota. Consistent with previous study, recipient mice recolonized with different microbiota did not showed obvious changed in levels of Scr, BUN and UA. However, mice colonized with HUA microbiota displayed more serious renal injury and higher UA levels compared to control mice after I/R. In contrast, mice recolonized with SMD treated microbiota exhibited attenuated renal injury and decreased UA levels when compared to HUA microbiota recipient mice after I/R. The decrease in UA levels seens to be a consequence of improved renal injury, not a direct effect of the SMD microbiota since no difference was seen in sham mice recolonized with different microbiota. Nevertheless, the causal relationship between the improvement of HUA and the modulation of gut microbiota is more likely a bidirectional interaction rather than a simple unidirectional causal link. On one hand, as shown in our study, a hyperuricemic environment may alter the structure and composition of gut microbiota. On the other hand, modulating the gut microbiota (e.g., with probiotics) has been shown to ameliorate HUA[35,36]. Moreover, levels of gut-derived uremic toxins (including IS and PC) were lower in mice recolonized with SMD-treated microbiota than in those receiving HUA microbiota. This provides additional evidence that the therapeutic effects of SMD on renal injury are mediated by the microbiota and their metabolites.

Both IS and PC are found to promote the progression of CKD[37,38]. To further investigate the mechanisms underlying the effects of IS and PC on renal injury, two types of renal tubular cells were utilized. Our results showed that IS induced an EMT-like process to promote renal fibrosis, which is consistent with previous studies[37]. Additionally, IS exhibited nephrotoxic effects through the induction of inflammation and acceleration

of cellular senescence[37,39]. Furthermore, it has been demonstrated that IS induces intestinal barrier injury through the impairment of mitophagy mediated by the IRF1-DRP1 axis[40]. PC is primarily conjugated to p-cresyl sulfate (PCS) within enterocytes. Similar to IS, PCS also promotes inflammation and renal fibrosis[41,42]. The primary structural difference between PCS and PC is the substitution of a hydroxyl group with a sulfate group, rendering PCS a hydrophilic compound. Therefore, PC appears to exhibit an enhanced ability to permeate the cell membrane and interfere with it functions, leading to increased biological toxicity relative to PCS. In this study, tubular cell proliferation was inhibited by PC. More importantly, PC treatment significantly accelerated tubular cell senescence in line with the results from the in vivo studies. Collectively, our findings suggest that the reduction of gut-derived uremic toxins, including IS and PC, may play a role in mediating the protective effects of SMD on HUA-induced renal injury.

In short, we investigated the therapeutic effects of SMD on renal injury induced by HUA using a uricase-deficient rat model. Mechanistically, SMD was observed to ameliorate gut dysbiosis and modulate bacterial metabolism of tryptophan and tyrosine, resulting in a decrease in gut-derived uremic toxins. This process ultimately inhibited renal fibrosis and tubular cell senescence in the kidneys of HUA rats (Fig. 12). This study provides new insights into the potential for therapy targeting the gut-kidney axis to address gut dysbiosis as a promising strategy for the treatment of HUA-related renal injury. The main limitation of the study is that we did not identify the key components of SMD that are responsible for the renal protective effects mediated by microbiota regulation. In addition, future studies designed with specific temporal analyses to track the sequential changes in both HUA and microbiota are essential.

Methods

Preparation and analysis of SMD

SMD was processed into formula granules by Jiangyin Tianjiang Pharmaceutical Co., Ltd. (lot: 2205312). SMD granule (12 g/packet) comprised Phellodendron amurense Rupr (10 g), Coix lacryma-jobi L. (10 g), Atractylodes lancea (Thunb.) DC. (5 g), Cyathula officinalis K.C.Kuan (5 g). As outlined in the 2020 edition of the Chinese Pharmacopoeia, issued by the Chinese Pharmacopoeia Commission, the UPLC fingerprint was observed at a wavelength of 203 nm. A sample preparation involved dissolving 500 mg of SMD powder in 15 mL of a 70% methanol solution, followed by filtration to facilitate subsequent UPLC-MS/MS analysis. The processes of sample preparation, extract analysis, and metabolite identification and quantification were conducted at GenChim Testing Co., Ltd. (Shanghai, China).

Animals and experimental design

The $UOX^{-/-}$ rats (male, 6 weeks) were generated by intercrossing $UOX^{+/-}$ rats obtained from Model Animal Research Center of Nanjing University. Wild-type littermates with genetically altered lines were used as controls. The rats were housed on a 12-h light-dark cycle at 24 ± 2°C. They had free access to food and water. The experiment was ethically approved by the Institution Animal Ethics Committee of Southern Medical University (No.SMUL202311021). The study design was as follows :

CTR group ($n = 8$): Wildtype rats were given purified water as drinking water.

MOD group ($n = 8$): $UOX^{-/-}$ rats were given purified water as drinking water.

L-SMD group ($n = 8$): $UOX^{-/-}$ rats were administered with low dose SMD (3 g/L) in drinking water for weeks. According to the body surface area conversion and the water intake of $UOX^{-/-}$ rats (60 ml/day), the low dose for mice (3 g/L) was approximately the clinical equivalent dose of SMD (12 g per day).

H-SMD group ($n = 8$): $UOX^{-/-}$ rats were administered with high dose SMD (6 g/L) in drinking water for weeks.

ALP group ($n = 8$): $UOX^{-/-}$ rats were administered with allopurinol (Aladdin, Shanghai, China) with a dose of 0.15 g/L in drinking water for 8 weeks.

To minimize the stress caused by prolonged oral gavage, the drugs were dissolved in purified water for the rats to drink ad libitum. The drinking water with or without drug was changed daily. After 8 weeks of the interventions, rats were anesthetized with sodium pentobarbital (50 mg/kg). Subsequently, feces, urine, blood, kidneys and colons tissue of rats were harvested and stored at -80 °C for subsequent analysis.

Fecal microbiota transplantation (FMT) was performed following an adapted protocol based on a previous study[15]. Specifically, 36 6-week-old male C57BL/6 J mice were treated orally once daily for five days with a combination of antibiotics-vancomycin (100 mg/kg), neomycin sulfate (200 mg/kg), metronidazole (200 mg/kg), and ampicillin (200 mg/kg)-to deplete their indigenous gut microbiota. On the evening of the fifth day, food was withdrawn while water remained freely available. Fresh fecal samples were aseptically collected from rats in the CTR, MOD, and H-SMD groups, pooled, and homogenized in pre-chilled sterile PBS (200 mg feces per mL). The suspension was centrifuged at 1000 rpm for 5 min at 4 °C, and the supernatant was collected. The resulting bacterial suspension was combined with an equal volume of 25% sterile glycerol to achieve a final concentration of 12.5% glycerol and stored at −80 °C until use. Each recipient mouse received 200 µl of the bacterial suspension via oral gavage daily for 14 consecutive days.

Renal ischemia/reperfusion (I/R) surgery was conducted by transiently clamping the bilateral renal artery. Mice were anesthetized with 1.25% 2,2,2-tribromoethanol (0.2 ml/10 g), and following laparotomy, both kidneys were exposed. The renal pedicle was clamped for 30 min using an atraumatic clip to induce ischemia, followed by 24 h reperfusion on a heating blanket. Mice were anesthetized with sodium pentobarbital (50 mg/kg) and kidneys and serum were collected for subsequent analysis.

Detection of serum UA, IS, PC and renal function indicators

Serum UA (BioAssay Systems, CA, USA), BUN, Scr and urine protein (Jiancheng, Nanjing, China) were detected using respective commercial kits. Urine sample was collected using metabolic cage. Urinary NAGL, β2-MG, KIM-1, CysC and RBP were dectected by ELISA quantitation kits (Boshen, Nanjing, China). Serum IS and PC were dectected by ELISA quantitation kits (Meimian, Jiangsu, China).

Detection of inflammation cytokines

Serum levels of MCP1, IL-1β, and IL-6 were quantified using ELISA kits according to the instructions (Boshen, Nanjing, China).

Histological analysis

The kidneys and distal colon tissues of rats were fixed in paraformaldehyde or carnoy's solution, embedded in paraffin and setioned into 5 µm thick slices. Standard protocols were followed for staining with haematoxylin and eosin (H&E), periodic acid schiff (PAS), masson trichrome and alcian blue (AB). Tubular injury was scored according to the previous study[15]. UA crystals in kidneys fixed in absolute ethanol were detected under polarized light. Colon injury was scored according to the previous study[43].

Immunostaining

Kidney sections embedded in paraffin were deparaffinized and subjected to antigen unmasking. And then they were blocked with 10% goat serum and immunostained overnight at 4 °C in a humidified chamber with antibodies targeting CD68 (1:200, GB113109, Servicebio) and collagen III (1:200, GB111629, Servicebio). Immunohistochemical staining was performed using DAB and counterstained with hematoxylin.

SA-β-gal staining

Senescent cells were stained using a SA-β-gal staining kit in accordance with the instructions (Beyotime, Shanghai, China).

Transmission electron microscopy (TEM)

Colon tissues were preserved in 2.5% (v/v) glutaraldehyde in PBS and processed according to standard protocols. Images were captured with a Hitachi transmission electron microscope from Japan.

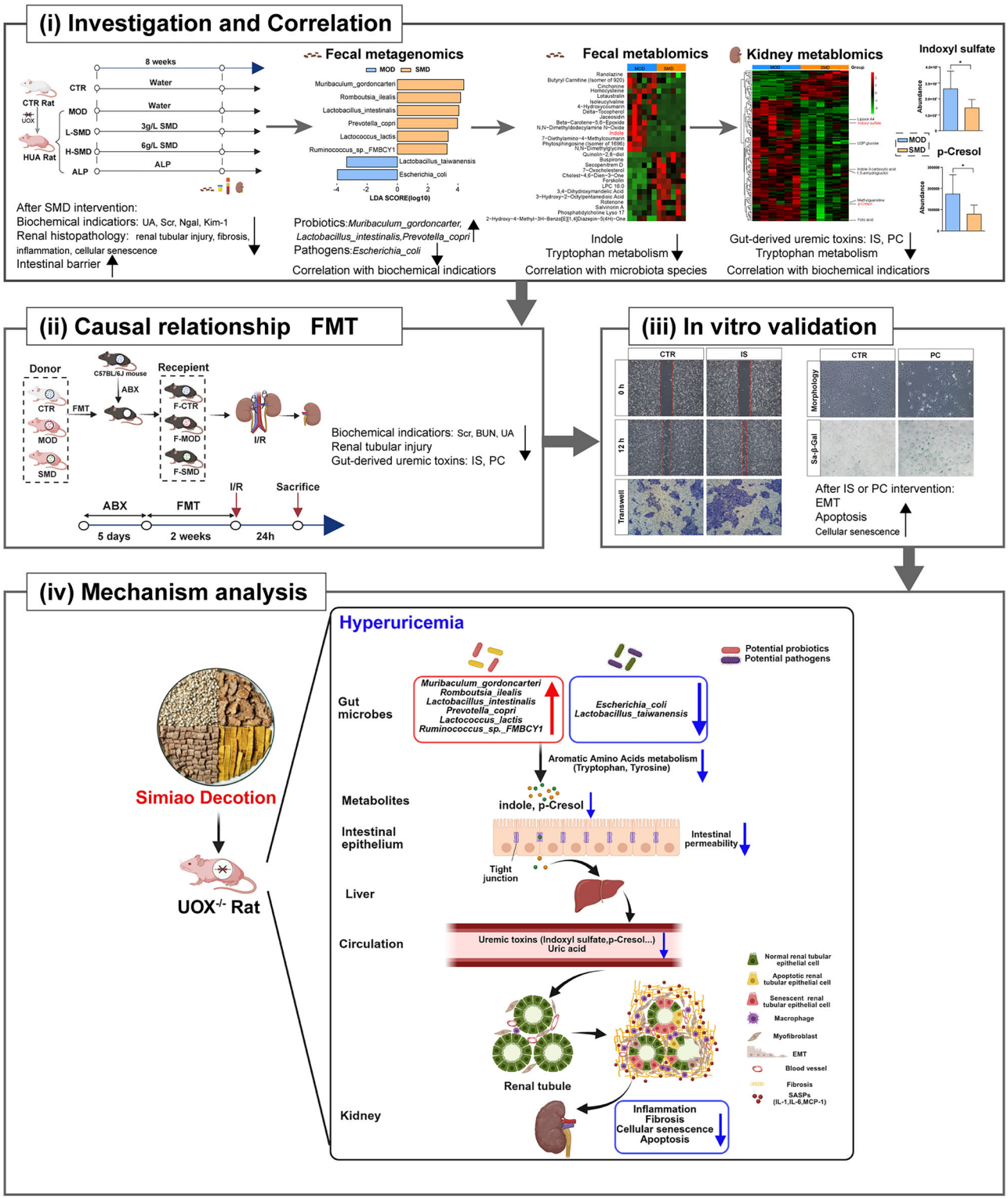

Fig. 12 | SMD alleviates HUA-induced renal injury through regulating gut dysbiosis and decreasing gut-derived uremic toxins. Flowchart depicting the integrated analyses of fecal metagenome, fecal and kidney metabolome, and fecal microbiota transplantation and in virtro experiments employed in this study. Mechanistically, SMD alleviates HUA-induced renal injury through regulating gut dysbiosis and decreasing gut-derived uremic toxins.

Western blot analysis

For the western blot analysis, 4 representative samples from each group of 8 were randomly selected for protein extraction and blotting. Proteins were extracted from kidney or colon tissues using RIPA lysis buffer and quantified with a BCA protein assay kit. Subsequently, Western blotting was carried out using the following antibodies: α-SMA (50513S, CST), β-actin (GB11001-100, Servicebio), caspase1 p20 (AF4005, Affinity), collagen IV (AF0510, Affinity), E-cadherin (14472S, CST), IL-1β (bs-6319R, Bioss), N-cadherin (14215S, CST), NLRP3 (bs-6655R, Bioss), occludin (GB111401-100, Servicebio), Smad2 (5339S, CST), TGF-β (ab66043, Abcam), $p16^{INK4A}$ (bs-55160R,Bioss), p21 (bs-55160R,Bioss), p53 (10442-1-AP,Proteintech),

ZO-1 (GB111402-100, Servicebio). Image J software was utilized for protein band analysis.

Metagenomic sequencing and taxonomic profiling

Genomic DNA was extracted from fecal samples using the E.Z.N.A.® Soil DNA Kit (Omega Bio-Tek, USA), with DNA concentration and purity assessed using Qubit4.0 and NanoDrop2000, respectively. The genomic DNA was fragmented to an average size of 300 bp for constructing paired-end libraries. Illumina paired-end libraries were subsequently generated using NovaSeq 6000 S4 Reagent Kit (Illumina, USA). Shallow shotgun sequencing was conducted using the Illumina NovaSeq platform with the NovaSeq Reagent Kits at Honsunbio Technology Co., Ltd. (Shanghai, China). The sequencing data has been uploaded to NCBI (Bioproject: *PRJNA1135458*).

The Illumina paired end reads underwent processing to eliminate adaptors and low-quality reads (defined as having a quality score of less than Q20, a length of less than 50 bp, or containing N bases). The Burrows-Wheeler Aligner was utilized to align reads to the rat reference genome (GCF_015227675.2_mRatBN7.2_genomic) using default parameters, with any matches related to reads and their paired reads being excluded. Taxonomic classification and abundance estimation of all metagenomic samples were conducted using Kraken 2 v2.1.2 and Bracken v2.8, employing a custom database comprising complete bacterial, archaeal, fungal, viral, protozoan, and human genomes, as well as UniVec core sequences sourced from RefSeq.

Statistical analysis and data visualization were conducted using R software. Principal coordinates analysis (PCoA) and PERMANOVA were performed utilizing the Bray-Curtis similarity matrices. The linear discriminant analysis (LDA) effect size (LEfSe) was conducted to dectermine differential abundance of species between groups (the default LDA score was 2). Predictions of functional category abundances were made using KEGG through PICRUSt based on operational taxonomic units (OTUs). Wilcoxon tests were conducted to assess variations in microbial community and functional diversity between two groups.

Metabolomic analysis

For feces metabolomic analysis, samples were weighed prior to metabolite extraction. The samples were freeze-dried and ground in a 2 mL Eppendorf tube with a 5 mm tungsten bead for 1 min at 65 Hz using a grinding mill. Metabolites were extracted using a chilled solvent mixture of methanol, acetonitrile, and water in a 2:2:1 volumetric ratio.This was followed by ultrasonic agitation for 1 h in an ice bath. The mixture was incubated at −20 °C for 1 h, followed by centrifugation at 14,000 *g* for 20 minutes at 4 °C. The supernatants were collected and subjected to vacuum concentration until dry. Metabolomics profiling was conducted using a UPLC-ESI-Q-Orbitrap-MS system with Q-Exactive Plus.

MS-DIAL processed the raw mass spectrometry data for peak alignment, retention time correction, and peak area extraction. Metabolite identification utilized accurate mass measurements (tolerance < 10 ppm) and MS/MS spectral data (tolerance < 0.02 Da), compared against databases such as HMDB, MassBank, other public repositories, and our proprietary standard library. Variables with over 50% nonzero measurements in any group were retained among the extracted-ion features.

The data was mean-centered using Pareto scaling prior to being applied in models built with partial least squares discriminant analysis (OPLS-DA) and evaluated via a 200-iteration random permutation test. Discriminating metabolites were identified using a statistically significant threshold based on VIP values from the OPLS-DA model and a two-tailed Student's t-test on normalized data. Metabolites with VIP ≥ 1.0 and $p < 0.05$ were considered statistically significant.

Metabolomic analysis of kidney tissues was performed as previously described[15].

Cell viability assay

The impact of IS (Sigma, USA) and PC (Selleck, USA) on cell viability was assessed using the MTT assay. Briefly, HK-2 and NRK-52E cells in the logarithmic growth phase were collected and plated into 96-well plates at a density of 10^5 cells per well. Cells were incubated with a concentration gradient of IS or PC at 37 °C and 5% CO_2 for 24, 48, and 72 h. Subsequently, 20 μL of MTT was introduced to each well for a period of 4 h, after which 150 μL of DMSO was added. The optical density (OD) of each well was measured at 570 nm using a microplate reader.

Scratch assay

To evaluate the migratory capacity of the cells, a scratch-wound assay was conducted. In brief, HK-2 and NRK-52E cells were cultured to confluence in a 6-well plate with 4×10^5 cells. Following the creation of a scratch using a sterile 200 μL pipet tip, the HK-2 and NRK-52E cells were incubated with 125 μM IS. The cells were then photographed at marked positions at both 0 and 12 h.

Transwell migration assay

HK-2 or NRK-52E cells were placed in the upper chamber of a transwell insert with 8.0 μm pores. 125 μM IS was added to the lower chamber after one hour, and cells were incubated for 24 h to promote migration. The insert was then removed, and a cell scraper was used to eliminate cells from the upper side of the membrane. The membranes were fixed with 4% paraformaldehyde, washed with PBS, and stained with Vectashield mounting medium containing DAPI. Images were captured using a microscope at 40× magnification (Olympus, Japan).

Flow cytometry

Cell apoptosis was assessed utilizing the Annexin V-FITC reagent. Following a 24-h treatment with PC, the cells were collected and subjected to two washes with PBS. Subsequently, the cells were resuspended and incubated with Annexin V-FITC and PI for 15 min at room temperature under dark conditions. The apoptosis rate was quantified using flow cytometry after adding 400 μl of binding buffer to each cell suspension.

Statistical analysis

The statistical analysis was performed using SPSS version 22.0 (Chicago, USA), with results expressed as means ± standard deviation (SD). The Student's *t* test was used to assess differences between two groups, while one-way ANOVA followed by the post hoc LSD test was employed for comparisons among multiple groups. A $p < 0.05$ indicated statistical significance.

Data availability

The shallow genome sequencing is available from the NCBI Sequence Read Archive (SRA) database (Bioproject: *PRJNA1135458*). The data for this study were available by contacting the corresponding author upon reasonable request.

Received: 29 May 2025; Accepted: 21 January 2026;
Published online: 31 January 2026

References

1. Zhang, M. et al. Prevalence of hyperuricemia among chinese adults: findings from two nationally representative cross-sectional surveys in 2015-16 and 2018-19. *Front. Immunol.* **12**, 791983 (2021).
2. Mortada, I. Hyperuricemia, type 2 diabetes mellitus, and hypertension: an emerging association. *Curr. Hypertens. Rep.* **19**(9), 69 (2017).
3. Kuwabara, M. et al. Uric acid is a strong risk marker for developing hypertension from prehypertension: a 5-Year Japanese Cohort Study. *Hypertension* **71**(1), 78–86 (2018).
4. Shi, Q. et al. Association between serum uric acid and cardiovascular disease risk factors in adolescents in America: 2001-2018. *Plos ONE* **16**(8), e254590 (2021).
5. Srivastava, A., Kaze, A. D., Mcmullan, C. J., Isakova, T. & Waikar, S. S. Uric acid and the risks of kidney failure and death in individuals with CKD. *Am. J. Kidney Dis.* **71**(3), 362–70 (2018).

6. Chou, Y. C. et al. Elevated uric acid level as a significant predictor of chronic kidney disease: a cohort study with repeated measurements. *J. Nephrol.* **28**(4), 457–62 (2015).
7. El, R. R. & Tallima, H. Physiological functions and pathogenic potential of uric acid: a review. *J. Adv. Res.* **8**(5), 487–93 (2017).
8. Jung, S. W., Kim, S. M., Kim, Y. G., Lee, S. H. & Moon, J. Y. Uric acid and inflammation in kidney disease. *Am. J. Physiol. Ren. Physiol.* **318**(6), F1327–40 (2020).
9. Yang, T., Richards, E. M., Pepine, C. J. & Raizada, M. K. The gut microbiota and the brain-gut-kidney axis in hypertension and chronic kidney disease. *Nat. Rev. Nephrol.* **14**(7), 442–56 (2018).
10. Chen, Y. Y. et al. Microbiome-metabolome reveals the contribution of gut-kidney axis on kidney disease. *J. Transl. Med.* **17**(1), 5 (2019).
11. Huang, Y. et al. The intestinal microbiota and metabolites in the gut-kidney-heart axis of chronic kidney disease. *Front. Pharm.* **13**, 837500 (2022).
12. Wang, H. et al. Perturbed gut microbiome and fecal and serum metabolomes are associated with chronic kidney disease severity. *Microbiome* **11**(1), 3 (2023).
13. Graboski, A.L. & Redinbo, M.R. Gut-derived protein-bound uremic toxins. *Toxins*. **12**, 590 (2020).
14. Wei, J. et al. Association between gut microbiota and elevated serum urate in two independent cohorts. *Arthritis Rheumatol.* **74**(4), 682–91 (2022).
15. Zhou, X. et al. Gut microbiota dysbiosis in hyperuricaemia promotes renal injury through the activation of NLRP3 inflammasome. *Microbiome* **12**(1), 109 (2024).
16. Guo, X. L. et al. Amelioration effects of alpha-viniferin on hyperuricemia and hyperuricemia-induced kidney injury in mice. *Phytomedicine* **116**, 154868 (2023).
17. Lu, M. et al. Fuling-Zexie formula attenuates hyperuricemia-induced nephropathy and inhibits JAK2/STAT3 signaling and NLRP3 inflammasome activation in mice. *J. Ethnopharmacol.* **319**(Pt 2), 117262 (2024).
18. Maiuolo, J., Oppedisano, F., Gratteri, S., Muscoli, C. & Mollace, V. Regulation of uric acid metabolism and excretion. *Int J. Cardiol.* **213**, 8–14 (2016).
19. Piani, F., Agnoletti, D. & Borghi, C. Advances in pharmacotherapies for hyperuricemia. *Expert Opin. Pharmacother.* **24**(6), 737–45 (2023).
20. Chen, L. et al. The efficacy and mechanism of chinese herbal medicines in lowering serum uric acid levels: a systematic review. *Front. Pharm.* **11**, 578318 (2020).
21. Peng, B. et al. Quercetin ameliorates hyperuricemic nephropathy through improving gut dysfunctions and decreasing gut bacteria-derived uremic toxins. *Phytomedicine* **143**, 156801 (2025).
22. Lin, X. et al. Simiao decoction alleviates gouty arthritis by modulating proinflammatory cytokines and the gut ecosystem. *Front. Pharm.* **11**, 955 (2020).
23. Hu, Q. H., Jiao, R. Q., Wang, X., Lv, Y. Z. & Kong, L. D. Simiao pill ameliorates urate underexcretion and renal dysfunction in hyperuricemic mice. *J. Ethnopharmacol.* **128**(3), 685–92 (2010).
24. Zhang, Y. et al. Simiao San alleviates hyperuricemia and kidney inflammation by inhibiting NLRP3 inflammasome and JAK2/STAT3 signaling in hyperuricemia mice. *J. Ethnopharmacol.* **312**, 116530 (2023).
25. Zeng, L. et al. Simiao pills alleviates renal injury associated with hyperuricemia: a multi-omics analysis. *J. Ethnopharmacol.* **333**, 118492 (2024).
26. Gong, W. et al. Brahma-related gene-1 promotes tubular senescence and renal fibrosis through Wnt/beta-catenin/autophagy axis.*Clin. Sci.***135**(15), 1873–95 (2021).
27. Luo, C. et al. Wnt9a promotes renal fibrosis by accelerating cellular senescence in tubular epithelial cells. *J. Am. Soc. Nephrol.* **29**(4), 1238–56 (2018).
28. Wang, W. J., Chen, X. M. & Cai, G. Y. Cellular senescence and the senescence-associated secretory phenotype: potential therapeutic targets for renal fibrosis. *Exp. Gerontol.* **151**, 111403 (2021).
29. Xu, J., Zhou, L. & Liu, Y. Cellular senescence in kidney fibrosis: pathologic significance and therapeutic strategies. *Front. Pharm.* **11**, 601325 (2020).
30. Liu, X. et al. Fecal microbiota transplantation restores normal fecal composition and delays malignant development of mild chronic kidney disease in rats. *Front. Microbiol.* **13**, 1037257 (2022).
31. Chang, H. W. et al. Prevotella copri and microbiota members mediate the beneficial effects of a therapeutic food for malnutrition. *Nat. Microbiol.* **9**(4), 922–37 (2024).
32. Kleerebezem, M. et al. Lifestyle, metabolism and environmental adaptation in Lactococcus lactis. *Fems Microbiol. Rev.* **44**(6), 804–20 (2020).
33. Li, G. & Young, K. D. Indole production by the tryptophanase TnaA in Escherichia coli is determined by the amount of exogenous tryptophan. *Microbiology* **159**(Pt 2), 402–10 (2013).
34. Pan, L. et al. Berberine ameliorates chronic kidney disease through inhibiting the production of gut-derived uremic toxins in the gut microbiota. *Acta Pharm. Sin. B* **13**(4), 1537–53 (2023).
35. Xu, Y. X. et al. Alistipes indistinctus-derived hippuric acid promotes intestinal urate excretion to alleviate hyperuricemia. *Cell Host Microbe* **32**(3), 366–81 (2024).
36. Zou, Z. P., Li, J. L., Zhang, Y. F., Zhou, Y. & Ye, B. C. Empowering probiotics with high xanthine transport for effective hyperuricemia management. *Gut Microbes* **16**(1), 2399213 (2024).
37. Lim, Y.J., Sidor, N.A., Tonial, N.C., Che, A. & Urquhart, B.L. Uremic toxins in the progression of chronic kidney disease and cardiovascular disease: mechanisms and therapeutic targets. *Toxins* **13**, 142 (2021).
38. Meijers, B. K. et al. p-Cresol and cardiovascular risk in mild-to-moderate kidney disease. *Clin. J. Am. Soc. Nephrol.* **5**(7), 1182–9 (2010).
39. Niwa, T. & Shimizu, H. Indoxyl sulfate induces nephrovascular senescence. *J. Ren. Nutr.* **22**(1), 102–6 (2012).
40. Huang, Y. et al. Indoxyl sulfate induces intestinal barrier injury through the IRF1-DRP1 axis-mediated mitophagy impairment. *Theranostics* **10**(16), 7384–400 (2020).
41. Gryp, T., Vanholder, R., Vaneechoutte, M. & Glorieux, G. p-Cresyl Sulfate. *Toxins*. **9**, 52 (2017).
42. Poveda, J. et al. p-cresyl sulphate has pro-inflammatory and cytotoxic actions on human proximal tubular epithelial cells. *Nephrol. Dial. Transpl.* **29**(1), 56–64 (2014).
43. Zhou, X. et al. Ginger extract decreases susceptibility to dextran sulfate sodium-induced colitis in mice following early antibiotic exposure. *Front. Med.* **8**, 755969 (2021).

Acknowledgements

This work was supported by the Joint Funds of National Natural Science Foundation of China [grant number U22A20365], National Natural Science Foundation of China [grant number 82274499, T2341019, 82405279], the Key Project of National Natural Science Foundation of China [grant number 81830117], the Guangzhou Science and Technology Plan Project [grant number 2024B03J1343], the Major scientific and technological project of Guangzhou Municipal Health Commission [grant number 20252D003], Guangdong Basic and Applied Basic Research Foundation, China [grant number 2023A1515110757], Dongguan social development technology program (High level hospital constructon project), China [grant number 20231800913372].

Author contributions

Xiaoshan Zhao and Yanyan Liu designed the study and supervised the project; Xinghong Zhou, Xiaoyu Liu, Baizhao Peng and Ying Yang completed the animal experiments, analyzed data and wrote the orignial manuscript; Hanqi Lu, Dexian Li, Yijian Deng and Zihao Jiang carried out metagenomic

and metabolomic analysis. Chuanghai Wu, Wen Fang and Yanting You completed the in vitro experiments and histological analysis. Hiu Yee Kwan provided technical assistance and revised the manuscript. All authors have read and approved the final version of the manuscript.

Competing interests
The authors declare no competing interests.

Additional information
Supplementary information The online version contains supplementary material available at https://doi.org/10.1038/s41522-026-00923-x.

Correspondence and requests for materials should be addressed to Xiaoshan Zhao or Yanyan Liu.